6-2010

Recovery of Carbon Dioxide from Flue Gases

Fahad Husain Al-Masabi

United Arab Emirates University
Deanship of Graduate Studies
M.Sc. Program in Petroleum Science & Engineering

RECOVERY OF CARBON DIOXIDE FROM FLUE GASES

By

Fahad Husain Al-Masabi

A Thesis Submitted to

United Arab Emirates University

In partial fulfillment of the requirements for the Degree of M.Sc. in

Petroleum Science & Engineering

Deanship of Graduate Studies

United Arab Emirates University

June, 2010

United Arab Emirates University
Deanship of Graduate Studies
M.Sc. Program in Petroleum Science & Engineering

Thesis Title

Recovery of Carbon Dioxide from Flue Gases

Author's Name

Fahad Husain Al-Masabi

Supervisor

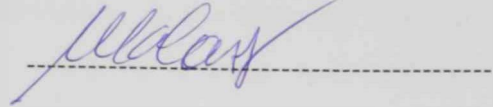| No	Name	Position
1	Dr. Marcelo Castier	Associate Professor of Chemical Engineering, Faculty of Engineering, United Arab Emirates University

Thesis of Fahad Husain Al-Masabi
Submitted in Partial Fulfillment for the Degree of
Master of Petroleum Science & Engineering

Chair of Examination Committee
Dr. Marcelo Castier
Chemical & Petroleum Engineering Department
United Arab Emirates University

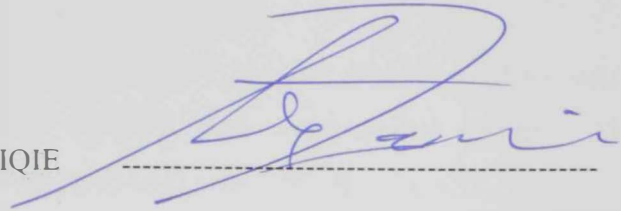External Examiner
Dr. Ricardo Macias-Salinas
Department of Chemical Engineering - ESIQIE
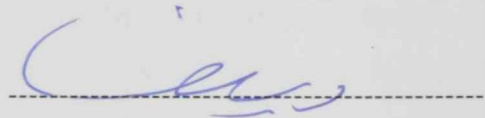National Polytechnic Institute, Mexico

Internal Examiner
Dr. Mohamed Younes El-Saghir Selim
Mechanical Engineering Department
United Arab Emirates University

Program Director
Prof. Abdulrazag Y. Zekri

-

Assoc. Dean for Scientific Research Studies
Dr. Ali H. Al-Marzouqi

United Arab Emirates University
2009/2010

Abstract

In this thesis, the modeling and simulation of the absorption of dilute CO_2 into falling film of aqueous solutions of a sterically hindered amine, 2-amino-2-methyl-1-propanol (AMP), was carried out using COMSOL Multiphysics Version 3.3. The operating cases were divided in two groups: (I) gas turbine operating cases (CO_2 3 mol %) and (II) boiler operating cases (CO_2 8.5 mol %). The key operating parameters for the studied cases are CO_2 partial pressure, operating temperature and amine concentration in the aqueous solution. The simulation focused on the following: (1) CO_2 Loading in aqueous AMP solution; (2) Required contact time to reach equilibrium; (3) pH of rich AMP aqueous solution; and (4) Total required interfacial area /circulated AMP aqueous solution.

The modeling was validated by solving the model under specific experimental operating conditions and comparing the predicted CO_2 loading with experimental results. The percentage error between the modeling and experimental was 3.97 %. The CO_2 loading in AMP aqueous solution approached one for some cases and is below 0.5 for other cases. High operating pressure, low operating temperature and low AMP aqueous concentration enhance CO_2 loading. The compression requirement for gas turbine flue gas was found to be higher than for boiler flue gas. The pH of rich AMP aqueous solution at maximum CO_2 loading was 8. The required contact time to reach equilibrium decreases with temperature increases. Finally, the results were utilized to estimate the lower bound to the size of a structured packed column as absorber for 100 MMSCFD total flue gas flow rate.

Table of Contents

List of Tables

List of Figures

Nomenclature

Roman letters

A_i	Interfacial area of the wetted column or pair parameters
C	AMP concentration
C_1^*	Interfac C o
c_i	Molar concentration of species i in falling film of AMP aqueous solution
d	Diameter of the wetted column
D_i	Binary diffusion coefficient for species i into falling film of AMP aqueous solution
$D_{CO2\text{-amine}}$	Diffusion coefficient of CO_2 into AMP aqueous solution
$D_{CO2\text{-water}}$	Diffusion coefficient of CO_2 into water
$D_{N2O\text{-amine}}$	Diffusion coefficient of N_2O into AMP aqueous solution
$D_{N2O\text{-water}}$	Diffusion coefficient of N_2O into water
g	Gravitational acceleration
G_p	Tower vapor loading (mass flow per unit area)
h	Height of the wetted column
H_1	Henry's constant of CO_2 into AMP aqueous solution
$H_{CO2\text{-amine}}$	Henry's constant of CO_2 into AMP aqueous solution
$H_{CO2\text{-water}}$	Henry's constant of CO_2 into water
$H_{N2O\text{-amine}}$	Henry's constant of N_2O into AMP aqueous solution
$H_{N2O\text{-water}}$	Henry's constant of N_2O into water
k_g	Gas phase mass transfer coefficient
k_{-i}	Backward reaction rate constant
K_1	Equilibrium constant
k_i	Forward reaction rate constant
M_g	Flue gas mass flow rate
M_l	AMP liquid mass flow rate
N_i	Combined molar flux vector for species i into falling film of AMP aqueous solution
P	Pressure
p_1	CO_2 partial pressure
p_1^*	Interfacial partial pressure of CO_2

Q_L	Volumetric liquid flow rate of AMP aqueous solution
R	Universal gas constant
$R_{i,net}$	Net reaction rate for species i
T	Temperature
V_{12}^E	Excess molar vo
V_i^o	Pure molar volumes of species i AMP (1) or water (2)
V_m	Molar v
vo	Volume percent
v_z	Vertical Velocity
v_z^*	Dimensionless velocity
$v_{z,max}$	Maximum velocity
$<v_z>$	Average velocity
wt%	Weight percent
x_i	Mole fractions of species i AMP (1) or water (2)
y_i	Mole fraction in vapor phase of species i

Greek letters

α	CO_2 loading in AMP aqueous solution (mol-CO_2 /mol-AMP)
δ	Falling film thickness
ΔH_f	Heat of Reaction
θ	Contact time of CO_2-AMP aqueous solution
μ	Dynamic viscosity
μ_m	Dynamic viscosity of AMP solution
ν	Component kinematic viscosity
ν_m	Kinematic viscosity of AMP solution
ρ	Density
ρ_g	Flue gas density
ρ_i^o	Pure densities of species i AMP (1) or water (2)
ρ_l	AMP liquid density
ρ_m	Densities of AMP aqueous solution

Abbreviations

MEA	Monoethanolamine
DGA	Diglycolamine
DEA	Diethanolamine
DIPA	Di-isopropylamine
TEA	Triethanolamine
MDEA	Methyl-diethanolamine
PFD	Process Flow Diagram
AMP	2-amino-2-methyl-1-propanol
IGCC	Integrated Gasification Combined Cycle
PTSA	Pressure and Temperature Swing Adsorption
TEPCO	Tokyo Electric Power Company
EOR	Enhanced Oil Recovery
[bmim][Tf$_2$N]	1-n-butyl-3-methylimidazolium bis[trifluoromethylsulfonyl]imide
[bmpy][Tf$_2$N]	1-n-butyl-1-methylpyrrolidinium bis(trifluoromethylsulfonyl)amide
[bmim][BF$_4$]	1-n-butyl-3-methylimidazolium tetrafluoroborate

CHAPTER I
INTRODUCTION

CHAPTER I
INTRODUCTION

The green house effect is that certain gases in the Earth's atmosphere let sunlight through to the Earth's surface, and then trap (absorb) outgoing infrared (long-wave) radiation, much in the same way that a greenhouse prevents heat from escaping through its glass panels. The gases that contribute most to the greenhouse effect are carbon dioxide (CO_2), methane (CH_4), nitrous oxide (N_2O), and fluorine compounds [1].
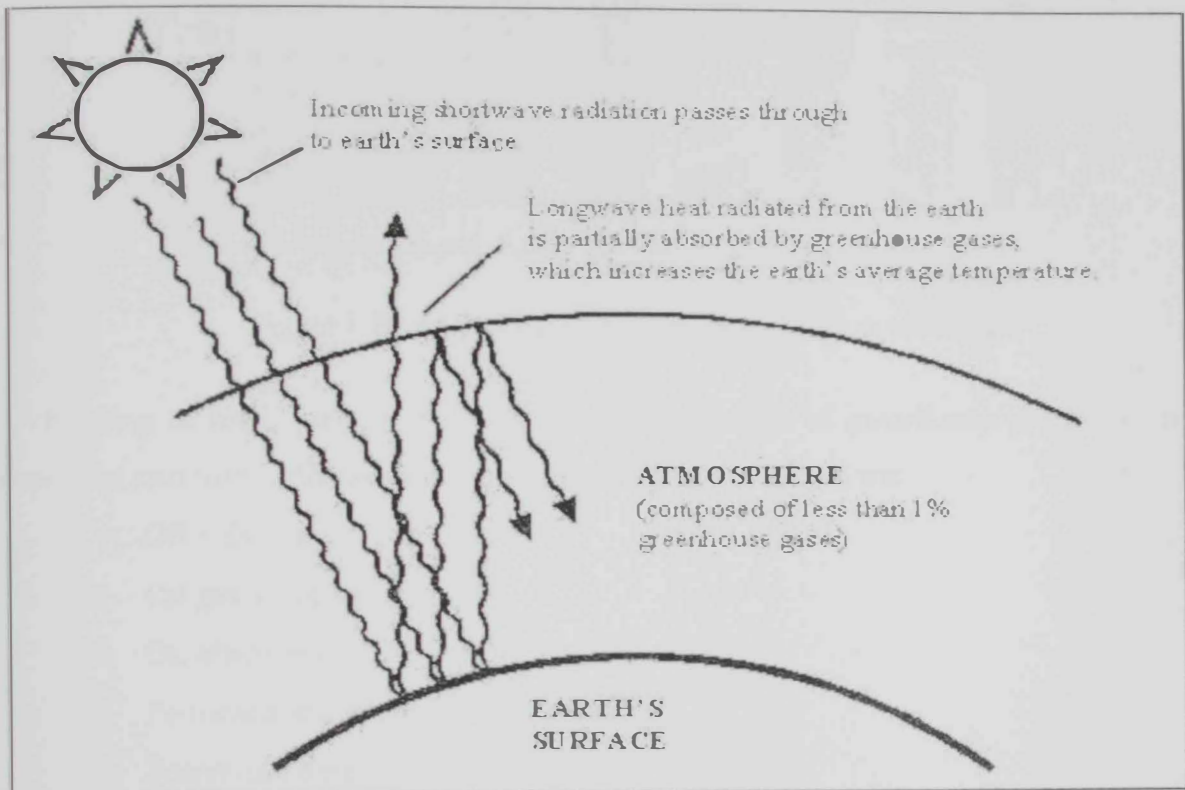
Figure 1-A: Green house effect phenomena [1]

The UAE's CO_2 emissions increased from 60,809,000 tonnes in 1990 to 94,163,000 tonnes in 2002. Presently, the country has one of the highest per capita commercial energy consumption rates in the world. Due to better technology and transition to more natural gas in power plants, emissions of CO_2 per capita have decreased. In 1990 the UAE emitted 32.6 tonnes CO_2 per person per year. In 2002 the figure had dropped to 25.1 tonnes per person per year, leav   U   26th, 2005 UAE became a member of United Nations Framework Convention on Climate Change (UNFCCC) after it signed the Kyoto Protocol.
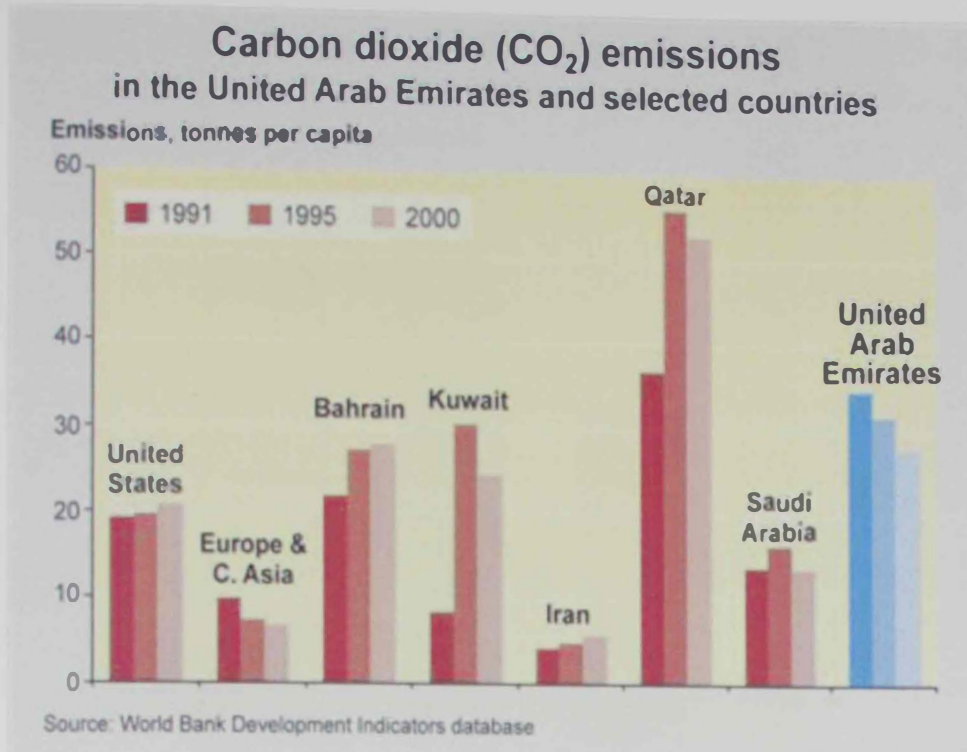
Figure 1-B: Annual CO_2 emissions for certain countries [2]

Burning of fossil fuels is the main cause of emissions of greenhouse gases. The most important stationary artificial sources of emissions in Abu Dhabi are:

- Oil refineries.
- Oil gathering centers.
- Oil platforms.
- Petrochemical and fertilizer plants.
- Power-and desalination plants [2].

There are five main techniques to recover CO_2 from flue gas: chemical and physical absorption, solid physical adsorption, cryogenic separation, membrane separation and alkaline salt based process. Each technique has some advantages and disadvantages related to operation, design and economics. The main objective of the thesis is to find an economical recovery technique, based on the results of simulations carried out by systematically changing several operating parameters for two case studies; gas turbine case study and boiler case study. Based on the results from simulations, the preliminary design of the absorber tower was carried out.

3

Key sources of CO_2 emissions
in Abu Dhabi Emirate

Emissions, tonnes per year

Source: ADNOC and Abu Dhabi Water and Energy Company
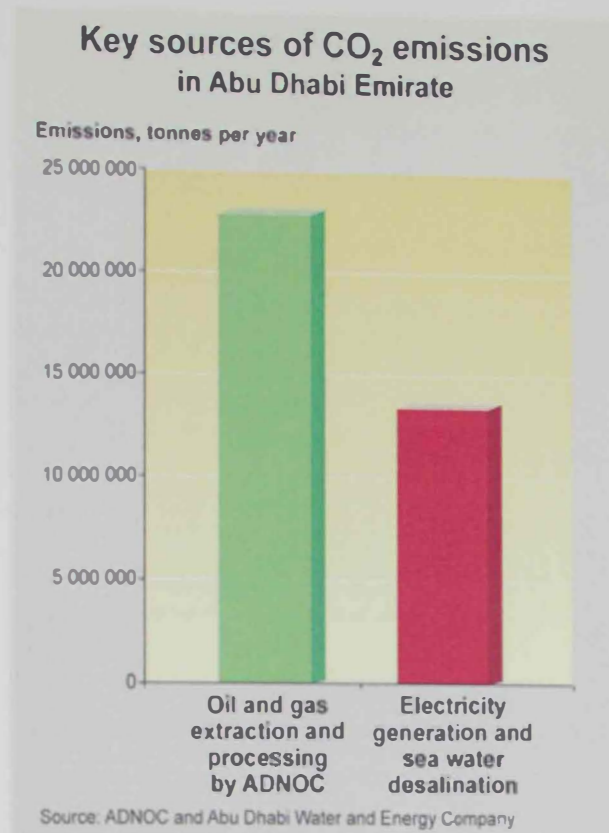
Figure 1-C: Key sources of CO_2 emissions in Abu Dhabi [2]

The report is organized into seven chapters, the first of them being a general introduction about the green house phenomena, comparing UAE yearly CO_2 emission with other countries and identifying the main sources of CO_2 emission in UAE. The second chapter highlights the main objective of this thesis which is to recover CO_2 in a practical and economic way. The third chapter studies the main techniques to recover CO_2 from flue gas which are chemical and physical absorption, solid physical adsorption, cryogenic separation, membrane separation and alkaline salt based process to screen them and select the most suitable one as thesis subject. The fourth chapter develops a model for the selected technique which is CO_2 absorption into amine aqueous solution. As simplification, the wetted column model was adopted. The fifth chapter presents the results of the modeling under different operating cases for gas turbine and boiler flue gases. The sixth chapter reports the results of calculation aimed at estimating the lower bound to the size of a structured packed column as absorber for 100 MMSCFD flue gas from gas turbine and boiler. Finally, the seventh chapter contains the conclusions and recommendations for future work.

4

CHAPTER II
OBJECTIVES

CHAPTER II
OBJECTIVES

The general objectives of this thesis are:

- To find an economical technique that recovers CO_2 with high purity by searching in scientific papers and reports;

- To identify and evaluate the available applied or proposed techniques to recover CO_2 by studying the principle, advantages and disadvantages of each;

- To develop a modeling with high degree of accuracy for the selected technique, capable of calculating the required parameters in a wide range of practical operating conditions.

The specific objectives of this thesis are:

- To apply the modeling for actual available applications in the United Arab Emirates (gas turbine and boiler);

- To optimize the operating condition required for the selected applications (gas turbine and boiler) by systematically changing the operating parameters.

- To reduce the operating cost by minimizing the requirement of compression and cooling of flue gas.

- To reduce the cost of pumping, the size of absorber and stripper columns, and the reboiler heat duty by maximizing the concentration of circulated AMP solution;

- To carry out preliminary design estimation of the absorber tower based on the optimization study.

CHAPTER III
LITERATURE REVIEW

CHAPTER III
LITERATURE REVIEW

3.1 Introduction

This chapter reviews and studies different separation processes used to recover CO_2 from flue gas. Each separation technique was studied and summarized from the viewpoint of design and operating issues and limitations. There are five main approaches to recover CO_2 from flue gas [3]:

1. Chemical and Physical Absorption
2. Solid Physical Adsorption – pressure swing and temperature swing adsorption
3. Low Temperature Distillation (Cryogenic Separation)
4. Membrane Separation
5. Alkaline Salt Based Process

3.2 Chemical Absorption

Alkanolamines are used to absorb CO_2 from flue gas streams. The chemical reactions that take place are exothermic. Different amines have different reaction rates. Alkanolamines can be divided into three groups:

1. Primary Amines whose members include monoethanolamine (MEA) and diglycolamine (DGA);
2. Secondary Amines whose members include diethanolamine (DEA) and di-isopropylamine (DIPA);
3. Tertiary Amines whose members include triethanolamine (TEA) and methyl-diethanolamine (MDEA) [3].

Table 3.2-A: Chemical formulas of alkanolamines [4]

Amines	Formula
MEA	$CH_2\,OH\,CH_2NH_2$
DGA	$CH_2NH_2\,CH_2O\,(CH_2)_2\,OH$
DEA	$(CH_3)_2\,CH_2\,CH_2NH$
DIPA	$CHNH\,CH\,(CH_2)_2\,(CH_3)_2\,(OH)_2$
TEA	$(CH_2)_5\,CH_2N\,(OH)_3$
MDEA	$CH_3N\,(CH_2)_4\,(OH)_2$

The standard process flow diagram (PFD) of Regenerable Alkanolamine Processes for recovery of CO_2 from flue gas is presented in Figure 3.2-A.

Figure 3.2-A: Standard PFD of regenerable alkanolamine process for recovery of CO_2 from flue gas [4]

Prior to entering to the absorber, the flue gas needs to be cooled by a direct contact cooler, as it is too hot, as well as treated to reduce the particulates and other impurities such as SO_x and NO_x to tolerable levels by adding caustic solution to cooling water. A feed blower provides the necessary pressure for the pretreated flue gas to overcome the pressure drop in the absorber [4]. The flue gas stream and liquid amine solution are contacted by countercurrent flow in an absorption tower. Usually, the flue gas to be scrubbed at the bottom of absorber, flows up, whereas the solvent enters the top of the absorber, flows down (contacting the flue gas), and gathers at the bottom. Dilution of the circulating amine with water is done to reduce viscosity of the circulating fluid [3]. The amine selectively absorbs CO_2 from the flue gas by chemically reacting with it. Small amounts of oxygen physically dissolve in the amine solution [4].

The rich amine solution, i.e. the liquid amine solution containing the absorbed flue gas, is pumped to the rich lean heat exchanger and then to a regeneration unit where it is heated and CO_2 is liberated [3]. A small portion of it is fed to a reclaimer, where heating to a higher temperature and addition of soda ash or caustic soda facilitates precipitation of any degradation byproducts and heat stable amine salts which are products of SO_X and NO_X reactions with the amine in the absorption column [4].

Regeneration of amine is often carried out at low pressure to enhance desorption of CO_2 from the amine solution. The CO_2-rich vapor stream from the top of the stripper is passed through a reflux condenser where it is partially condensed resulting in the separation of a CO_2 stream and a condensate stream which is fed back to the stripper. The main function of the condenser is to recover all carryover amine solution [4].

The hot lean amine solution then flows through a heat exchanger (shell side) where it is contacted with the rich amine solution (tube side) from the contact tower. Then lean amine solution is returned to the flue gas contact tower [3].

The detailed design of the unit shown in Figure 3.2-A depends on many factors, among which the type of alkanolamine used to absorb CO_2. There are three key aspects to be considered: (1) the solubility of CO_2 in the aqueous alkanolamine solution, which affects the amount of CO_2 that can be absorbed per unit amount of solvent; (2) the rate of absorption which is a kinetic aspect that affects absorption equipment size; (3) the heat of absorption and desorption, as it affects the amount of energy required to recover the solvent for recycling. The next section discusses key aspects of the main types of alkanolamines that are either used industrially or are being considered for use, according to the literature [3].

3.2.1 Primary Amines (MEA)

Primary amines such as MEA are the traditional solvent of choice for carbon dioxide absorption. MEA is the least expensive of the alkanolamines, has the lowest molecular weight, and has the highest theoretical absorption capacity for carbon dioxide. This theoretical upper absorption capacity of MEA is not realized in practice due to corrosion problems [3]. As result, uninhibited MEA solutions are generally limited by corrosion problems to about 15-20 wt% MEA. The low MEA concentration raises the reboiler duty. For example, the reboiler duty increases 20% when the MEA concentration decreases from 30 to 15 wt%. The required pump power increases even more. Some corrosion inhibitors in conjunction with a quantitative oxygen and NO_X removal system allow the MEA concentration to be raised to 25-30 weight percent [5].

In addition, MEA has the highest vapor pressure of any of the alkanolamines and high solvent carryover during absorption and regeneration. In order to reduce solvent losses, a water wash of the purified gas stream is usually required.

Furthermore, MEA reacts irreversibly with minor impurities such as COS, CS_2 and SO_X resulting in solvent degradation. Foaming of the absorbing liquid MEA due to the build-up of impurities can also be a concern [3].

For MEA absorber systems, the absorption and desorption rates are reasonably high. However, the column packing represents a significant cost, and its energy consumption is also significant for flue gas treatment. In addition, the stripping temperature should not be too high. Otherwise, dimerization of carbamate may take place, deteriorating the absorption capability of MEA [3].

In a commercial process, concentrations of MEA up to 30-wt% have been employed successfully to remove 80% - 90% of the carbon dioxide from the feed gas. The process has been used to treat flue gas, however, some cooling and compression of the gas is required to operate the system. Another commercial process, which uses 20% MEA with inhibitors, is also offered for flue gas treatment [3].

The Econamine FG process uses an inhibited 30 wt% MEA solution. These features allow the widespread use of carbon steel and give the process the lowest stripper reboiler steam demand among all of the well-established commercial processes. It can recover 85-95% of the CO_2 in the flue gas and produces a 99.95+% pure CO_2 product (dry basis). The inhibitor not only tolerates oxygen and NO_X-containing flue gas, but also requires oxygen to maintain its activity. The process can be used with SO_X-containing flue gas after SO_2 scrubbing. The additional SO_2 scrubbing returns an environmental benefit. The Econamine FG process is not applicable to reducing gas streams, for instance streams containing large amounts of carbon monoxide and hydrogen, on streams that contain more than 1 ppm hydrogen sulfide, or on streams that have less than 1 vol% oxygen. The process is applicable to pressurized gas streams, but the full commercial advantage of this process lies in atmospheric pressure applications [5].

Kerr-McGee/ABB Lummus Global has licensed four units that use 15-20 wt% MEA to recover CO_2 from coal-fired flue gas. The plant capacities vary between 180 and 720 tonnes/day [5].

3.2.2 Secondary and Tertiary Amines

Secondary amines have advantage over primary amines in that their heat of reaction with carbon dioxide is lower. This means that secondary amines require less heat in the regeneration step than primary amines. Tertiary amines have slower reaction with carbon dioxide than primary and secondary amines thus require higher circulation rate of liquid to remove carbon dioxide compared to primary and secondary amines. A major advantage of tertiary amine is their lower heat requirements for carbon dioxide desorption from the carbon dioxide containing solvent. Table 3.2.2-A displays data for the heat of reaction between three amines and carbon dioxide [3].

Table 3.2.2-A: Heat of reaction between Amines and CO_2 [3]

Amine	MEA (Primary)	DEA (Secondary)	MDEA (Tertiary)
ΔH_f for carbon dioxide (BTU / lbm CO_2)	820	650	577

Tertiary amines show a lower tendency to form degradation products than primary and secondary amines, and are more easily regenerated. In addition, tertiary amines have lower corrosion rates compared to primary and secondary amines [3].

The energy required to regenerate amine is an important factor for amine selection. For this type of application the regeneration energy is referred to as reboiler heat duty. The reboiler heat duty is essentially a sum of the energy utilized for three main purposes: raising the temperature of CO_2-loaded solution to the boiling point, breaking the chemical bonds between CO_2 and absorption solvent, and generating water vapor to establish an operating CO_2 partial pressure needed for CO_2 stripping. The level of reboiler heat duty relates directly to the quantity of CO_2 stripped from the regeneration column and the quality of lean solution fed back to the absorption column. That is, a higher heat duty results in a larger amount of CO_2 product and a leaner solution leaving the regeneration column [6].

Figure 3.2.2-A shows the reboiler heat duty of MEA, DEA, and MDEA at 0.50 mol/mol rich-CO_2 loading and 4.0 kmol/m^3 alkanolamine concentration. As the reboiler heat duty increases, the lean-CO_2 loading decreases and finally stabilizes at a minimum value (equilibrium condition). The minimum lean-CO_2 loading is specific to each alkanolamine, i.e., 0.22 mol/mol for MEA, 0.06 mol/mol for DEA, and 0.02 mol/mol for MDEA. The minimum lean-CO_2 loading is an indication of the liquid circulation rate. A higher minimum lean-CO_2 loading suggests a greater liquid circulation rate. MEA requires a greater liquid

circulation rate than DEA and MDEA to capture a given amount of CO_2. MEA appears to require the highest reboiler heat duty followed by DEA and MDEA [6].
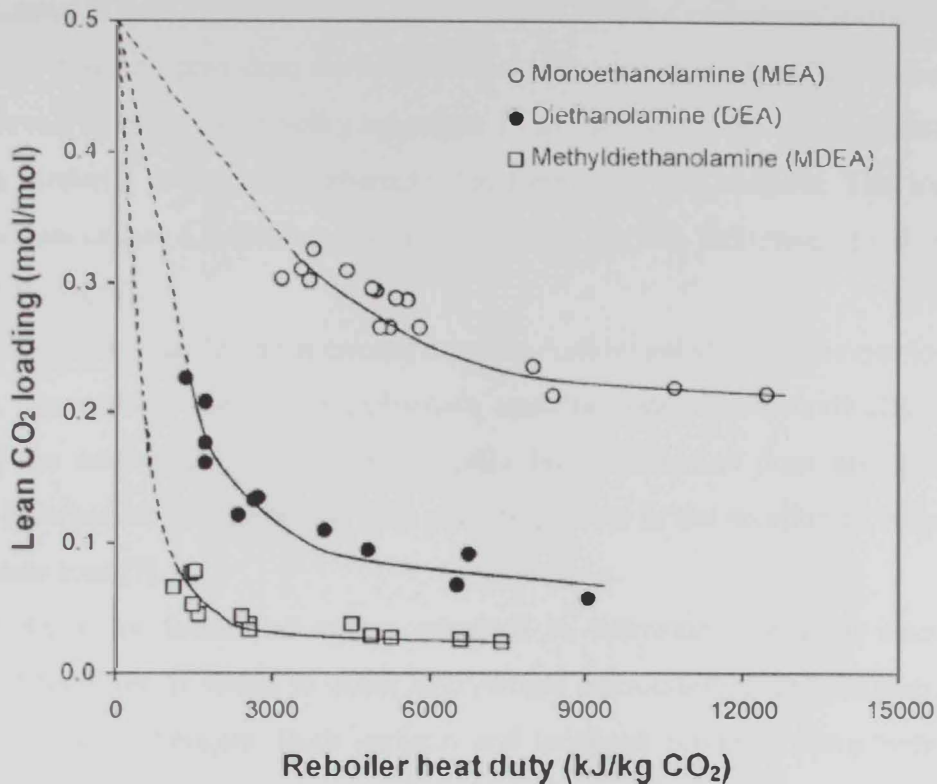
Figure 3.2.2-A: Reboiler heat duty of MEA, DEA and MDEA solutions [6]

Tertiary amines show a lower tendency to form degradation products than primary and secondary amines, and are more easily regenerated. In addition, tertiary amines have lower corrosion rates compared to primary and secondary amines [3].

It may be pointed out that corrosion has been a serious issue in amine processes. In general, alkanolamines themselves are not corrosive to carbon steel; the dissolved CO_2 is the primary corroding agent. As such, the alkanolamines indirectly influence corrosion rate due to their absorption of CO_2. The observed corrosivity of alkanolamines to carbon steel is generally in the order (Primary Amines > Secondary Amines > Tertiary Amines) [3].

3.2.3 Sterically Hindered Amines

Primary and secondary amines react rapidly with CO_2 to form carbamate with a stoichiometric loading of 0.5 mol of CO_2/mol of amine. The CO_2 loading in the sterically hindered amine approaches a value of 1.0 mol of CO_2/mol of amine as in the case of the tertiary amine MDEA, while the reaction rate constant for CO_2 is much higher than that for CO_2 in MDEA [7].

13

The idea of using hindered amines is based on the reaction rates of the acid gases with different amine molecules. In the case of CO_2 removal, the capacity of the solvent can be greatly enhanced if one of the intermediate reactions, i.e. the carbamate formation reaction can be slowed down by providing steric hindrance to the reacting CO_2. This hindrance effect can be achieved by attaching a bulky substitute to the nitrogen atom of the amine molecule [3]. With a hindered amine, the carbamate can form, but it is unstable. The formation of stable carbamate causes a stoichiometric absorption or loading limitation of 0.5 mol of CO_2 per mole of amine [8].

In addition to slowing down the overall reaction, bulkier substitutes give rise to less stable carbamates. By making the amine carbamate unstable, one can theoretically double the capacity of the solvent [3]. Since the sterically hindered amine does not form a stable carbamate, bicarbonate and carbonate ions may be present in the solution in larger amounts than carbamate ions [7].

One of the main factors of amine selection is corrosion rate as it causes serious operational difficulties. It seems to occur everywhere particularly in regenerators, reboilers, and rich-lean heat exchangers. Both uniform and localized corrosion have been observed, depending on the design and the way in which the equipment is operated. The major parameters contributing to the corrosion process are dissolved carbon dioxide (CO_2), dissolved oxygen (O_2), alkanolamines, degradation products, temperature, and solution velocity. The average corrosion rates in the AMP (2-amino-2-methyl-1-propanol) system are lower than those in the MEA system when absorption of pure CO_2 and absorption of a mixture of 52 % CO_2 and 48 % air (see Figure 3.2.3-A and Figure 3.2.3-B) [9].

An industrial company and electric power company in Japan developed a hindered amine called KS-1 as an MEA replacement for flue gas applications. KS-1 has a lower circulation rate (due to its higher lean to rich CO_2 loading differential), lower regeneration temperature ($110^{\circ}C$), and 10-15% lower heat of reaction with CO_2. It is non-corrosive to carbon steel (less than 5 mpy) at $130^{\circ}C$ in the presence of oxygen. A second sterically hindered amine, AMP, may have similar properties to KS-1 [5].
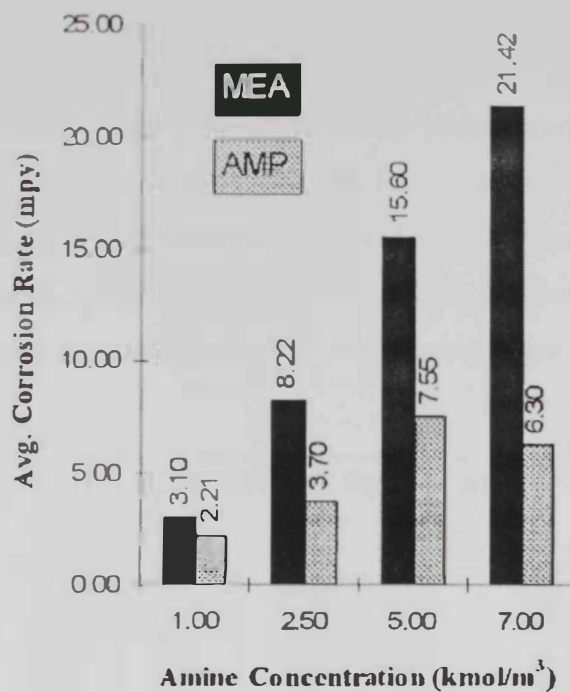
Figure 3.2.3-A: Corrosion rates in MEA and AMP solutions saturated with pure CO_2 [9]
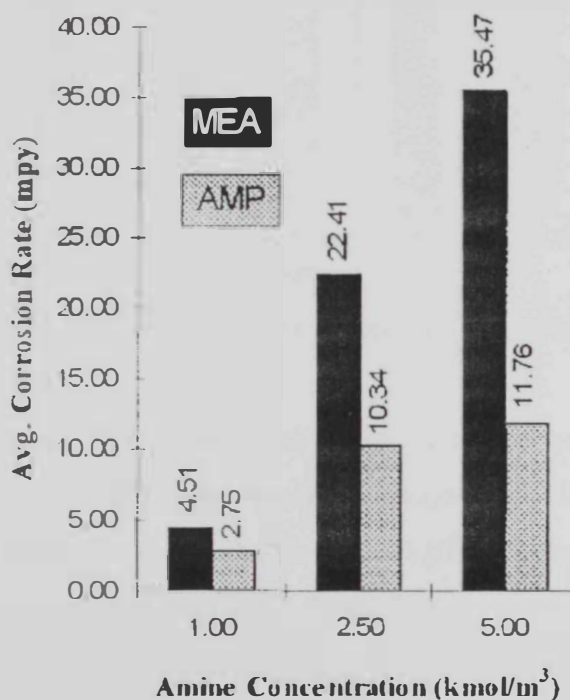
Figure 3.2.3-B: Corrosion rates in MEA and AMP solutions saturated with a mixture of 52 % CO_2 and 48 % air [9]

Figure 3.2.3-C shows the regeneration efficiency for each amine at 1.0 kmol/m³ alkanolamine concentration and regeneration temperature 383 K. It is apparent that MEA gave the lowest regeneration efficiency of 88.3% in the first cycle, whereas, AMP offered the highest performance of 98.3%. With this figure, the regeneration performance can be ranked

in the following order: AMP > MDEA > DETA > DEA > MEA. This performance order is similar to that of the regeneration performance in the second cycle. Figure 3.2.3-C also shows that the regeneration efficiency of MEA has the most pronounced drop between cycles, decreasing from 88.3% in the first cycle to 77.6% in the second cycle. However, AMP maintains the highest regeneration efficiency of 97.8%. This is because AMP has a molecular structure of sterical hindering, which results in the sterically hindered amines being easily regenerated and shows better degradation resistance, in comparison to other alkanolamines [10].
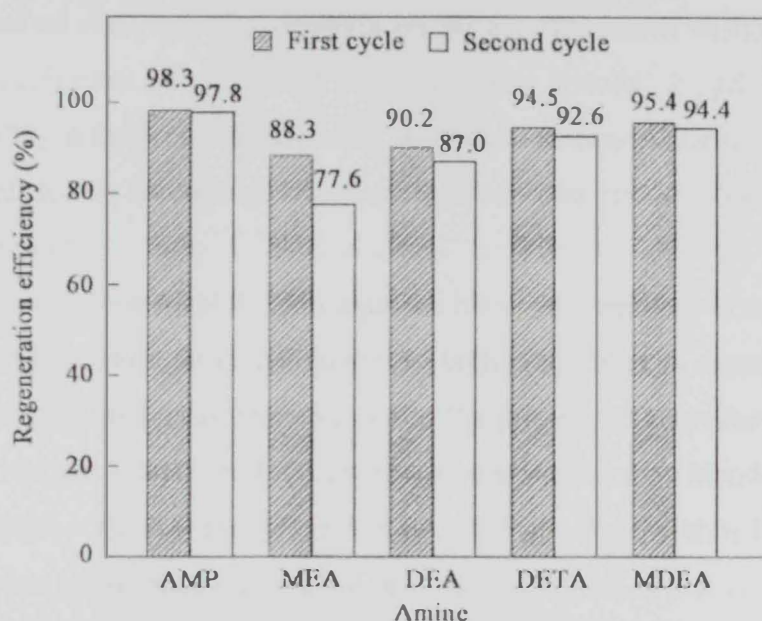
Figure 3.2.3-C: Amine solution regeneration efficiency [10]

Vapor-liquid equilibria of four absorbents were measured using 1 L equilibrium apparatus. Table 3.2.3-A shows the experimental measured CO_2 loading of absorbent at different operating temperatures 40°C for absorber and 120°C for stripper. The CO_2 partial pressure for both absorber and stripper is 9.8 kPa [11].

Table 3.2.3-A: CO_2 loading of absorbent [11]

Amine	Concentration (kmol/m³)	CO_2 Loading (mol CO_2 / mol amine)		Effective CO_2 Loading (mol CO_2 / mol amine)
		Absorber Condition	Stripper Condition	
MEA	1	0.606	0.204	0.402
KS-1	1	0.801	0.231	0.57
AMP	1	0.755	0.158	0.597
DEA	1	0.614	0.137	0.477

As shown in Table 3.2.3-A, the AMP effective CO_2 loading is higher than that of KS-1 at the above absorber and stripper conditions.

3.2.4 Blending of Amines

The goal when using an aqueous mixture of alkanolamines is to maximize the desirable qualities of the individual alkanolamines, that is, to retain much of the high absorption rates of primary or secondary alkanolamines, to offer low regeneration costs, and to decrease both corrosion and circulation rates [8].

The realization of such benefits depends on proper equipment design, which requires knowledge of equilibrium solubility of CO_2 in amine blends. In addition, equilibrium solubility of the CO_2 in aqueous alkanolamine solutions determines the minimum circulation rate of the solvent. It also determines the maximum concentration of CO_2 can be left in the regenerated solution [7].

A blended amine solvent, which is an aqueous blend of a primary or a secondary amine with a tertiary or a hindered amine, combines the higher equilibrium capacity of the tertiary or hindered amine with the higher reaction rate of the primary or secondary amine. (AMP + MEA + H_2O) and (AMP + DEA + H_2O) appear to be attractive new blended amine solvents in addition to (MDEA + MEA + H_2O) and (MDEA + DEA + H_2O) blends for the gas-treating processes. The lower vapor pressure of DEA and the fact that it is less corrosive than MEA makes the DEA based blended amine solvents more attractive in principle than MEA-based ones [7].

3.3 Physical Absorption

The physical absorption of CO_2 depends on temperature and pressure and is favored by high partial pressure of CO_2 and by low temperature. The physical solvents are then regenerated by either heating or pressure reduction. The advantage of this method is that it requires relatively little energy, but CO_2 must be at high partial pressure. For this reason, it is suitable for recovering CO_2 from Integrated Gasification Combined Cycle (IGCC) systems where the exhaust CO_2 would leave the gasifier at elevated pressures. Typical physical solvents are Selexol (dimethylether of polyethylene glycol) and Rectisol (cold methanol) [3].

Selexol has been used since 1969 to sweeten natural gas, both for bulk CO_2 removal and H_2S removal. Absorption takes place at low temperature ($0 - 5^{\circ}C$). Desorption of CO_2 from the rich Selexol solvent can be accomplished either by pressure reduction or by stripping

(with air, inert gas or steam). The low absorption temperature used requires that the lean solvent be returned to the absorber via a refrigeration unit [3].

Rectisol has mainly been used to treat synthesis gas, hydrogen and gas streams and removes most impurities. Rectisol process separates CO_2 from mixture of H_2, CO and CO_2. In general, the solvent is chilled methanol but other solvents are also available for special applications [3].

Recent studies about using ionic liquids to recover CO_2 show that they may be attractive due to their good features: reasonable thermal stability, negligible vapor pressure, and high CO_2 solubility. Ionic liquids with imidazolium-based cations are found to be the best to recover CO_2 from flue gas. Table 3.3-A shows the Henry's constants of CO_2 in some ionic liquids. By comparing the Henry's constant of CO_2 in ionic liquids with amine, the CO_2 solubility in ionic liquids is typically 10 times higher than in amines. However, the viscosity of ionic liquids is high: for example, [bmim][BF_4] is 40 times more viscous as compared to 30% MEA at 33°C. High viscosity of ionic liquids decreases the diffusion of CO_2 and absorption capacity and increases the time to reach equilibrium condition (maximum absorption). Blending of ionic liquid with water or some common organic solvents like polyethylene glycol reduces the mixture viscosity and consequently enhances the rates of absorption and desorption. Another option to enhance CO_2 absorption is to blend alkanolamines with ionic liquids in order to combine their advantages, i.e. negligible vapor pressure, high thermal stability and low heat capacity of ionic liquids, and fast capture kinetics and low viscosity of alkanolamines. Figure 3.3-A presents the CO_2 absorption of some conventional aqueous amine solutions (30 wt% MEA or MDEA) at 40°C, 1-n-butyl-3-methylimidazolium tetrafluoroborate [bmim][Tf_2N] at 30°C and task specific ionic liquids ([Am-im][BF4] and [Am-im][DCA]) at 30°C. Observing Figure 3.3-A, the chemical absorption by alkanolamines is better than ionic liquids. Regeneration of ionic liquids can be carried out by vacuum separation, by applying heat or by bubbling nitrogen through the absorbent. However, task specific ionic liquids mixed with amine require vacuum heating [12].

Table 3.3-A: Henry's constants of CO_2 in ionic liquids [12]

Ionic liquid		H_{CO_2}			
		25°C		40°C	
Short Name	Full name	bar	$m^3.Pa/mol$	bar	$m^3.Pa/mol$
[bmim][Tf_2N]	1-n-butyl-3-methylimidazolium bis[trifluoromethylsulfonyl]imide	34.3	62	45	81
[bmpy][Tf_2N]	1-n-butyl-1-methylpyrrolidinium bis(trifluoromethylsulfonyl)amide	33	60	41	74
[bmim][BF_4]	1-n-butyl-3-methylimidazolium tetrafluoroborate	56	101	73	132
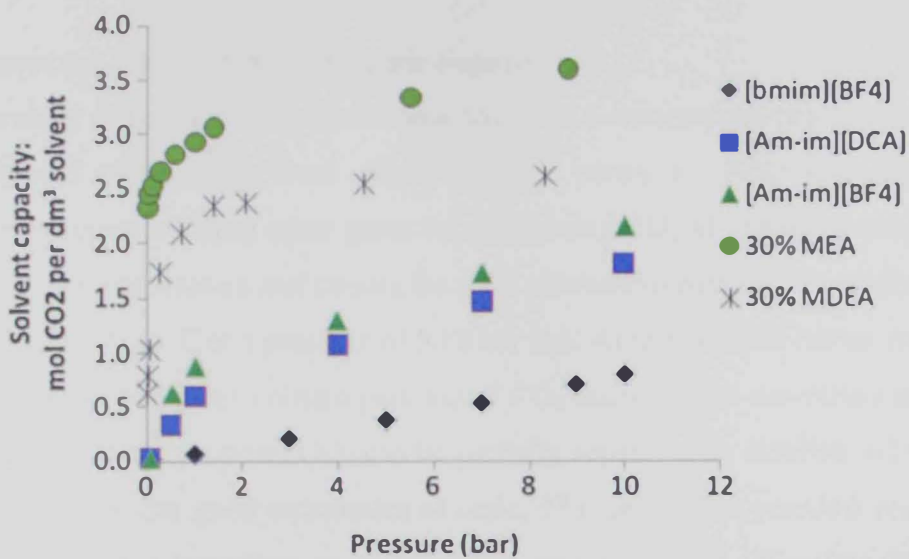
Figure 3.3-A: Molar CO_2 loads in solvent volume for some conventional amines and ionic liquids [12]

3.4 Solid Physical Adsorption

An adsorption process consists of two major steps: adsorption and desorption. The technical feasibility of a process is stated by the adsorption step, whereas desorption step controls its economic feasibility. Strong attraction of an adsorbent for removing CO_2 from the flue gas is essential for an effective adsorption step. The stronger the attraction, the more difficult it is to desorb the flue gas impurity and the higher the energy consumed in regenerating the adsorbent for reuse in the next cycle [3].

The main advantage of physical adsorption over chemical or physical absorption is its simple and energy efficient operation and regeneration, which can be carried out with a pressure swing or temperature swing cycle [3]. A combination process of pressure and

19

temperature swing adsorption (PTSA) has been tested at the bench scale and pilot-scale levels by Tokyo Electric Power Company (TEPCO) & Mitsubishi Heavy industries, respectively. Bench scale PTSA tests selected an adsorbent zeolite for having a high capacity and selectivity. However, this pilot-scale test from a power station burning coal/oil mix and a flue gas with a concentration of 10.8% (higher than the gas power plant flue gas) and CO_2 generated a recovery of 90% CO_2. Using PTSA compared to PSA reduced the power consumption required for separation by 11%. Under the current state of technology, adsorption is yet not considered attractive for large scale separation of CO_2 from flue gases because of the capacity and CO_2 selectivity of available adsorbents is low [13].

3.5 Low Temperature Distillation (Cryogenic Separation)

Low temperature distillation (cryogenic separation) is a commercial process commonly used to liquefy and purify CO_2 from relatively high purity (> 90%) sources. In this technology, CO_2 is separated from other gases by condensing CO_2 at cryogenic temperature, based on lowering the temperature and raising the total pressure to equilibrium condition. The triple point of CO_2 is − 56.6°C at a pressure of 5.18 bar abs. At temperature lower than that of the triple point, it is not possible to obtain pure liquid CO_2 making such conditions unsuitable for distillation. Above the triple point CO_2 can be partially separated by distillation [13].

Distillation generally has good economies of scale. This method is practical considering where there is a high concentration of CO_2 in the waste gas [3]. Therefore, cryogenic distillation is generally used commercially for purification of CO_2 from streams that already have high CO_2 concentration (> 50 %). It is unusual to use cryogenic distillation for dilute CO_2 streams such as flue gas from boiler and gas turbine as the amount of energy required for refrigeration is uneconomic for this condition [13]. The other disadvantage of this process is the necessary removal of components that have freezing points above normal operating temperatures to avoid freezing and eventual blockage of process equipment [3].

For post combustion flue gases, the waste streams contain water and other trace combustion by-products such as NO_x and SO_x several of which must be removed before the stream is introduced to the low temperature section [3].

These tend to make cryogenic process less economical than others in separating CO_2 from flue gas. But, it might appear more attractive when combined with other CO_2 capture techniques especially when high purification and liquefaction are required [13].

3.6 Membrane Separation

Membranes suffer from both the cost of compression and heat exchange to obtain a high pressure feed and in that they produce an impure CO_2 product. For example, Separex membrane systems are currently offered by UOP for feed pressures starting at 2851 kPa. There are currently no commercial applications of membranes for recovery of CO_2 from flue gases, though they have been used in large EOR projects to recycle CO_2 from the associated gas. The presence of fly ash and the effects of trace components such as SO_X, NO_X, HCl, and HF are also potential complications [13].

Membranes for gas separation are usually formed as hollow fibers arranged in the tube-and-shell configuration, or as flat sheets, which are typically packaged as spiral-wound modules. Compared to absorption separation, the advantages of the membrane process are:

1) It does not require a separating agent, thus no regeneration is required;

2) It is compact and lightweight. So, it is more suitable for offshore applications.

3) Modular design allows optimization of process arrangement by using multi-stage operation; and

4) Low maintenance requirements because there are no moving parts in the membrane unit [5].

A number of solid polymer membranes are commercially available for the separation of CO_2 from gas streams, primarily for natural gas sweetening. These membranes selectively transmit CO_2 versus CH_4. The driving force for the separation is pressure differential across the membrane. As such, compression is required for the feed gas in order to provide the driving force for permeation, and the separated CO_2 is at low pressure and requires additional compression to meet pipeline pressure requirements. The required energy for gas compression is significant when a very high pressure is required [5].Membranes cannot usually achieve high degrees of separation, so multiple stages and/or recycle of one of the streams is necessary. This leads to increased complexity, energy consumption and cost [13].

3.7 Alkaline Salt Based Process

Alkaline salts of weak acids were proposed and tested to recover CO_2 from flue gas. The conventional used alkaline salts in industry are sodium and potassium salts. The primary advantages of alkaline salt based process are low solvent cost and negligible solvent degradation. However, the method has many disadvantages, [3]:

- Alkaline salt solution reacts slowly with CO_2.
- Required regeneration heat is much higher than alkanolamine process.
- Vacuum is required during the stripping regeneration.
- Vapor recompression may be required.
- Alkaline salt solution is limited by salt precipitation.
- Foaming was highlighted to have significant impact of alkaline salt process.
- Corrosion inhibitor is required to mitigate the server corrosion rate for carbon steel.

3.8 Summary of the Literature Review

Chemical absorption by aqueous amine currently is most economic and suitable method for CO_2 recovery from gas turbine exhaust (post combustion) where the pressure is almost atmospheric, resulting in a low CO_2 partial pressure. Criticism of this method includes aspects such as high energy consumption during regeneration, corrosion, and thermal stability. Despite such criticisms, absorption by amine solution has been used for many years in industry for natural gas sweetening. The absorption-stripping system is particularly interesting as it can operate continuously in closed cycle. Among different types of amines (primary, secondary and tertiary amines), sterically hindered amines are found to have higher absorption rates, lower circulation rates, lower regeneration temperature and lower corrosion impact against carbon steel.

CHAPTER IV
MODELING OF CO_2 ABSORPTION INTO AMINE SOLUTION FALLING FILM

CHAPTER IV

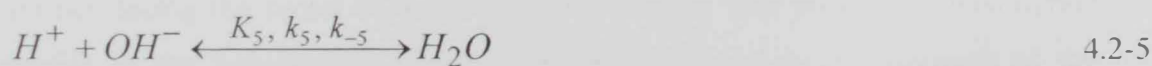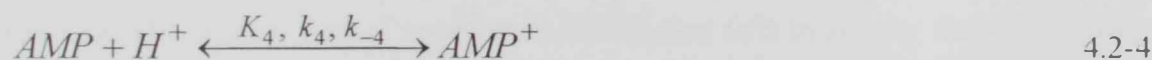# MODELING OF CO_2 ABSORPTION INTO AMINE SOLUTION FALLING FILM

4.1 Introduction

Based on the literature review, AMP was selected to be studied in this thesis due to its good features. The objective was to develop a model for the absorption of CO_2 in an AMP solution. An immediate solution for this modeling problem using HYSYS Version 3.2, commonly utilized by chemical process industries, was not possible because AMP is not included in its Amine Package. Moreover, HYSYS is unable to simulate the reaction-diffusion problem characteristic of this absorption process. This problem can be solved in full detail in a computational fluid dynamics program, but the complexities associated with simulating a packed reactive column are high. As simplification, a wetted column model was adopted, which was implemented and solved in COMSOL Multiphysics Version3.3.

4.2 Reaction Scheme and Reaction Mechanism

The reactions between amines and carbon dioxide (CO_2) have been studied and examined. CO_2 reacts in aqueous amine systems indirectly as bicarbonate and directly (carbamate reaction).

$$CO_2 + AMP + H_2O \xleftrightarrow{K_1, k_1, k_{-1}} AMP^+ + HCO_3^- \qquad 4.2\text{-}1$$

$$CO_2 + OH^- \xleftrightarrow{K_2, k_2, k_{-2}} HCO_3^- \qquad 4.2\text{-}2$$

$$HCO_3^- \xleftrightarrow{K_3, k_3, k_{-3}} H^+ + CO_3^{2-} \qquad 4.2\text{-}3$$

$$AMP + H^+ \xleftrightarrow{K_4, k_4, k_{-4}} AMP^+ \qquad 4.2\text{-}4$$

$$H^+ + OH^- \xleftrightarrow{K_5, k_5, k_{-5}} H_2O \qquad 4.2\text{-}5$$
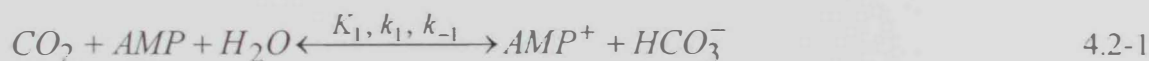
where:

K_i : Equilibrium constants for the reactions 4.2-1, 4.2-2, 4.2-3, 4.2-4 and 4.2-5

k_i : Forward reaction rate constants for the reactions 4.2-1, 4.2-2, 4.2-3, 4.2-4 and 4.2-5

k_{-i} : Backward reaction rate constants for the reactions 4.2-1, 4.2-2, 4.2-3, 4.2-4 and 4.2-5

All the reactions are reversible. Reactions 4.2-1 and 4.2-2 have finite reaction rates. Reactions 4.2-3, 4.2-4, and 4.2-5 are assumed to reach equilibrium instantaneously [14]. COMSOL Multiphysics expects rate constants for all reactions. Approximation to the assumption that reactions 4.2-3, 4.2-4 and 4.2-5 are instantaneous, the reaction constants k_3, k_4 and k_5 are assumed to be equal to 1000 times k_2.

Base-catalyzed bicarbonate formation is found to be a likely mechanism for all amine bases. Direct formation of bicarbonate species from carbamate species is found to be unlikely [15]. Primary and secondary amines can form carbamates. However, tertiary and hindered amines cannot form stable carbamates because of low stability constants which causes carbamates to readily undergo hydrolysis forming bicarbonate and releasing free amine that can again react with CO_2 [16]. 2-amino-2-methyl-1-propanol (AMP) is the hindered form of MEA. The bulky group attached to the tertiary carbon atom of AMP inhibits the formation of stable carbamate ions [17]. Since the sterically hindered amine like AMP, does not form a stable carbamate, bicarbonate and carbonate ions may be present in the solution in larger amounts than the carbamate ions [16].

For convenience, the concentrations of chemical species are renamed as follows:

$$c_1 = [CO_2] \qquad c_2 = [AMP] \qquad c_3 = [AMP^+]$$
$$c_4 = [HCO_3^-] \qquad c_5 = [OH^-] \qquad c_6 = [CO_3^{-2}]$$
$$c_7 = [H^+]$$

4.3 Modeling Description

The modeling describes CO_2 absorption into amine based on the principle of a falling laminar film that involves diffusion and reaction processes for CO_2 mass transfer in aqueous solution. The laminar film of aqueous amine solution falls in annular flow with a free liquid surface facing the center of a tube. Falling laminar film provides a well-defined velocity profile in the liquid phase in order to obtain an analytical estimation of the diffusion boundary layer. The gas is introduced in the middle of the tube and is absorbed through the free surface of the liquid. The contact surface between the gas and the liquid is confined to the free surface inside of the tube. Figure 4.3-A shows a schematic of the falling film at the tube wall.

When modeling a stationary convection-diffusion process that has negligible convective transport in one direction (in this case, the radial direction) and negligible diffusive transport in the other direction (in this case, the axial direction), it is possible to reformulate the

convection-diffusion equation by switching the axial derivative to a time derivative. To be able to do so, the velocity field along the axial direction must not change. This enables to reduce one space dimension of the problem, making it a 1D problem (x, time). In COMSOL Multiphysics. this is a "pseudo-2D equation" [18].
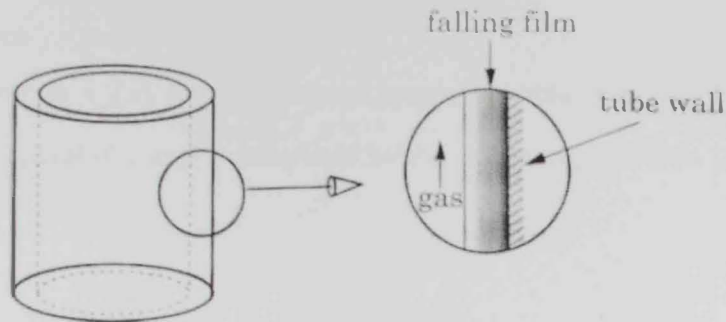
Figure 4.3-A: Schematic of the falling film at the tube wall [18]

4.4 Modeling Assumptions

In order to formulate the model, the following assumptions are considered:

1. Steady state;
2. Laminar flow in the liquid phase;
3. Isothermal system;
4. Newtonian fluid;
5. Constant density and viscosity;
6. The liquid flows downward under the influence of pressure difference and gravity;
7. The radius of the tube is large enough, in comparison to the thickness of the falling film to neglect effects of curvature in the tube;
8. The tube length is very large with respect to the tube radius so that "end effects" can be ignored;
9. The contribution of diffusion to the flux of species is negligible in the direction of the convective flow, i.e., in the vertical direction;
10. There is no slip at the wall;
11. All the reactions are considered elementary;
12. The thickness of fluid layer is much smaller than cylinder radius in order to use Cartesian coordinates;
13. CO_2 is assumed to be pure in gas phase to eliminate mass transfer resistance in the gas phase;

14. All the reactions are reversible. Reactions 4.2-1 and 4.2-2 have finite reaction rates. Reactions 4.2-3, 4.2-4, and 4.2-5 are assumed to reach equilibrium instantaneously;

15. The ratio of diffusion coefficients to that of CO_2 is about 0.3 for all other species (AMP, AMP+, HCO_3^-, OH^-, CO_3^{-2} and H^+).

4.5 Momentum Balance

The velocity distribution $v_z(x)$ for the laminar, incompressible flow of a Newtonian fluid in a long vertical tube is parabolic and is described by the following equation [19]:

$$v_z = \frac{\rho g \delta^2}{2\mu}\left[1 - \left(\frac{x}{\delta}\right)^2\right]$$ 4.5-1

where:

v_z : Vertical velocity (m/s)

μ : Dynamic viscosity (Pa.sec)

ρ : Density (kg/m^3)

g : Gravitational acceleration (m/sec^2)

δ : Falling film thickness (m)

The radius of the tube is assumed large enough, in comparison to the thickness of the falling film, to neglect effects of curvature in the tube and assume the segment as straight line. The following figure illustrates the type of velocity distribution predicted by Equation 4.5-1.
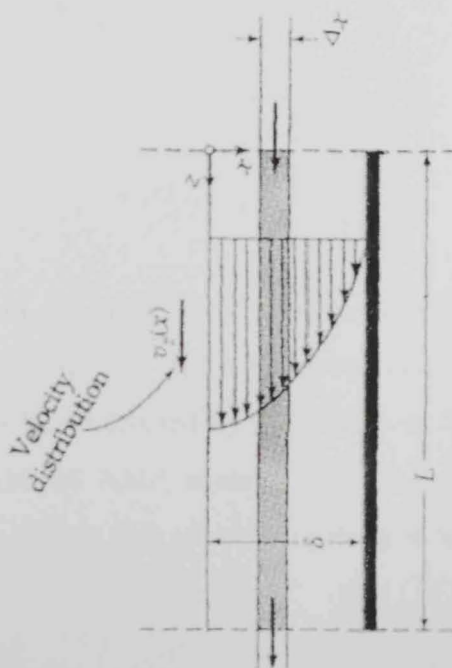

Figure 4.5-A: Velocity distribution for the falling film [10]

27

The maximum velocity $v_{z,\,max}$ is the velocity at gas-liquid interface ($x = 0$)

$$v_{z,max} = \frac{\rho g \delta^2}{2\mu}$$

4.5-2

Therefore

$$v_z = v_{z,max}\left[1-\left(\frac{x}{\delta}\right)^2\right]$$

4.5-3

The average velocity $<v_z>$ over a cross section of the film is obtained as follows;

$$<v_z> = \frac{\int_0^W \int_0^\delta v_z\, dxdy}{\int_0^W \int_0^\delta dxdy} = \frac{1}{\delta}\int_0^\delta v_z\, dx$$

$$= \frac{\rho g \delta^2}{2\mu}\int_0^1\left[1-\left(\frac{x}{\delta}\right)^2\right]d\left(\frac{x}{\delta}\right)$$

$$= \frac{\rho g \delta^2}{3\mu} = \frac{2}{3}v_{z,max}$$

4.5-4

$$v_{z,max} = 1.5 <v_z>$$

4.5-5

Therefore

$$v_z = 1.5 <v_z>\left[1-\left(\frac{x}{\delta}\right)^2\right]$$

4.5-6

Then dimensionless velocity ($v_z^* = \frac{v_z}{<v_z>}$) can be determined as follows [19]:

$$v_z^* = 1.5\left[1-\left(\frac{x}{\delta}\right)^2\right]$$

4.5-7

4.6 Mass Balance

Diffusion into a falling liquid film (gas absorption) is considered as forced convection mass transfer, in which viscous flow and diffusion occur under such conditions that the velocity field can be assumed to be unaffected by the diffusion. Specifically, the absorption of CO_2 by a laminar falling film of AMP aqueous solution is considered. Figure 4.6-A illustrates absorption of CO_2 into falling film of AMP aqueous solution.

28
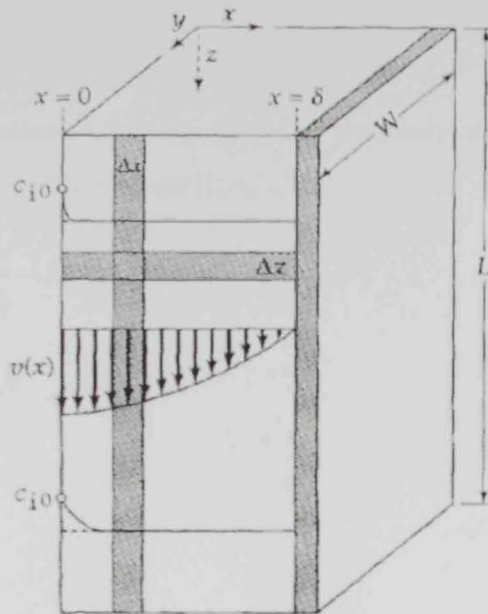
Figure 4.6-A: Absorption of CO_2 into falling film of AMP aqueous solution [19]

The flue gas flows upward the wetted column starting from the bottom and AMP aqueous solution flows downward starting from the top.

In order to carry out the mass balances, a mass balance equations was formulated for each component i, which not only diffuses and flows but also reacts at a net reaction rate $R_{i.net}$.

The combined molecular diffusion and convective molar flux of each species can be obtained from Equation 4.6-1

$$N_i = -D_i \frac{\partial c_i}{\partial x} + c_i v_z \qquad 4.6\text{-}1$$

where:

N_i: Combined molar flux vector for species i into falling film of AMP aqueous solution (mol/ m^3.sec)

D_i: Binary diffusion coefficient for species i into falling film of AMP aqueous solution (m^2/sec)

c_i: Molar concentration of species i in falling film of AMP aqueous solution (mol/m^3)

Based on the previous assumptions in section 4.4, the diffusion-reaction can be formulated using the following equation

$$\nabla.N_i - R_{i,net} = 0 \qquad 4.6\text{-}2$$

By adding Equations 4.6-1 and 4.6-2, the following equation results [19]:

$$-D_i \frac{\partial^2 c_i}{\partial x^2} + v_z \frac{\partial c_i}{\partial z} - R_{i,net} = 0 \qquad\qquad 4.6\text{-}3$$

We can rewrite Equation 4.6-3 by using the transformation $z = <v_z> t$ which is valid under the constant velocity profile assumption.

$$-D_i \frac{\partial^2 c_i}{\partial x^2} + v_z \frac{\partial c_i}{\partial (<v_z> t)} - R_{i,net} = 0$$

$$-D_i \frac{\partial^2 c_i}{\partial x^2} + \frac{v_z}{<v_z>} \frac{\partial c_i}{\partial t} - R_{i,net} = 0$$

Since $v_z^* = \dfrac{v_z}{<v_z>}$

$$-D_i \frac{\partial^2 c_i}{\partial x^2} + v_z^* \frac{\partial c_i}{\partial t} - R_{i,net} = 0 \qquad\qquad 4.6\text{-}4$$

The dimensionless velocity Equation 4.5-7 obtained from momentum balance can be added to Equation 4.6-4. This gives us the final system of equations in our domain [18]:

$$-D_i \frac{\partial^2 c_i}{\partial x^2} + 1.5\left[1 - \left(\frac{x}{\delta}\right)^2\right] \frac{\partial c_i}{\partial t} - R_{i,net} = 0 \qquad\qquad 4.6\text{-}5$$

According to the Reactions 4.2-1, 4.2-2, 4.2-3, 4.2-4 and 4.2-5, the net rate reaction of each species i can be formulated as following

$$R_{1,net} = -k_1 c_1 c_2 + k_{-1} c_3 c_4 - k_2 c_1 c_5 + k_{-2} c_4 \qquad\qquad 4.6\text{-}6$$

$$R_{2,net} = -k_1 c_1 c_2 + k_{-1} c_3 c_4 - k_4 c_2 c_7 + k_{-4} c_3 \qquad\qquad 4.6\text{-}7$$

$$R_{3,net} = k_1 c_1 c_2 - k_{-1} c_3 c_4 + k_4 c_2 c_7 - k_{-4} c_3 \qquad\qquad 4.6\text{-}8$$

$$R_{4,net} = k_1 c_1 c_2 - k_{-1} c_3 c_4 + k_2 c_1 c_5 - k_{-2} c_4 - k_3 c_4 + k_{-3} c_7 c_6 \qquad\qquad 4.6\text{-}9$$

$$R_{5,net} = -k_2 c_1 c_5 + k_{-2} c_4 - k_5 c_7 c_5 + k_{-5} \qquad\qquad 4.6\text{-}10$$

$$R_{6,net} = k_3 c_4 - k_{-3} c_7 c_6 \qquad\qquad 4.6\text{-}11$$

$$R_{7,net} = k_3 c_4 - k_{-3} c_7 c_6 - k_4 c_2 c_7 + k_{-4} c_3 - k_5 c_5 c_7 + k_{-5} \qquad\qquad 4.6\text{-}12$$

The thermodynamic relationship between the forward and backward reaction rate constants is shown in Equation 4.6-13.

$$k_{-i} = \frac{k_i}{K_i} \qquad\qquad 4.6\text{-}13$$

4.7 Boundary Conditions

The boundary conditions to solve the set of partial differential equations of the model are:

- **B.C.1:** At $z = 0$, the concentrations of the chemical species are equal to their liquid bulk concentrations, i.e.,

$$c_i = c_i^o (i = 1, 2,....., 7) \quad at \ z = 0 \qquad 4.7\text{-}1$$

In this project, the amine liquid solution is assumed to be free of dissolved CO_2. So, C_i is equal to zero except C_2 [19].

- **B.C.2:** At $x = 0$ (gas-liquid interface), the fluxes of non-volatile chemical species are equal to zero, which leads to $\frac{\partial c_i}{\partial x} = 0$ for all i except i = 1 (CO_2). For the volatile component (CO_2), the mass transfer rate in the gas near the interface is equal to the mass transfer rate in the liquid near the interface

$$- D_1 = \frac{\partial c_1}{\partial x} = k_g \left[p_1 - H_1 c_1 \right] \quad at \ x = 0 \qquad 4.7\text{-}2$$

where:

k_g : Gas phase mass transfer coefficient ($mol/m^3.sec$)

p_1 : CO_2 partial pressure (pa)

H_1 : Henry's constant of CO_2 into AMP aqueous solution ($pa.m^3/mol$)

For the case of pure CO_2 in the gas phase, the interfacial partial pressure of CO_2, p_1^*, is the same as the bulk partial pressure of CO_2, P_1, and there is negligible mass transfer resistance in the gas phase. Equation 4.7-2 can be reduced to [16]:

$$c_1 = c_1^* = \frac{P_1}{H_1} \quad at \ x = 0 \qquad 4.7\text{-}3$$

- **B.C. 3:** At $x = \delta$ the diffusion of any chemical species on the wall is zero, which leads to [19]:

$$\frac{\partial c_i}{\partial x} = 0 \quad at \ x = \delta \qquad 4.7\text{-}4$$

31

4.8 Physiochemical properties and model parameters

4.8.1 Reactions Equilibrium Rate Constants

The values of the equilibrium constants K_i for the Reactions 4.2-1, 4.2-2, 4.2-3, 4.2-4 and 4.2-5 are determined from the following correlations [14]:

$$\log_{10}\left(\frac{1}{K_5}\right) = 8909.483 - \frac{142613.6}{T} - 4229.195 \log_{10}(T) + 9.7384\ T - 0.0129638\ T^2$$
$$+ 1.15068 \times 10^{-5}\ T^3 - 4.602 \times 10^{-9}\ T^4 \qquad 4.8\text{-}1$$

$$\log_{10}\left(\frac{K_2}{K_5}\right) = 179.648 + 0.019244\ T - 67.341 \log_{10}(T) - \frac{7495.441}{T} \qquad 4.8\text{-}2$$

$$\log_{10}(K_3) = 6.498 - 0.0238\ T - \frac{2902.4}{T} \qquad 4.8\text{-}3$$

$$\ln\left(\frac{K_4}{K_5}\right) = \frac{-7261.78}{T} - 22.4773 \ln(T) + 142.58612 \qquad 4.8\text{-}4$$

$$K_1 = \frac{K_2\ K_4}{K_5} \qquad 4.8\text{-}5$$

where:

T: Temperature (K)

The corresponding units of K_1 to K_5 according to equations 4.8-1, 4.8-2, 4.8-3, 4.8-4 and 4.8-5 are shown in Table 4.8.1-A

Table 4.8.1-A: the units of K_1 to K_5

	K_1	K_2	K_3	K_4	K_5
Unit	Dimensionless	$m^3/kmol$	$kmol/m^3$	$m^3/kmol$	$m^6/kmol^2$

Table 4.8.1-B shows the calculated values of reaction equilibrium constants at different temperatures

Table 4.8.1-B: Calculated values of reaction equilibrium constants at different

temperatures

T (K)	K_1	K_2 (m^3/mol)	K_3 (mol/m^3)	K_4 (m^3/mol)	K_5 (m^6/mol^2)
293.15	2916	56505	4.17E-08	7591546	147106733
298.15	2198	41116	4.65E-08	5335509	99806074
303.15	1656	30117	5.12E-08	3798603	69101825
308.15	1246	22195	5.56E-08	2736519	48747712
313.15	937	16449	5.98E-08	1992960	34991666
318.15	704	12254	6.36E-08	1466176	25527575
323.15	528	9175	6.69E-08	1088864	18907817
328.15	396	6903	6.97E-08	815863	14205802
333.15	297	5218	7.20E-08	616462	10817652

4.8.2 Kinetic Rate Constants of the Forward and Backward Reactions

The reaction rate constants of the first and second reactions (finite reaction rates) are determined from the following correlations [14]:

$$k_1 = 1.399 \times 10^7 \exp\left(-\frac{24261}{RT}\right) \qquad 4.8\text{-}6$$

$$\log_{10}(k_2) = 13.635 - \frac{2895}{T} \qquad 4.8\text{-}7$$

where:

T: Temperature (K)

k_1: Forward reaction kinetic rate constant of Reaction 4.2-1 (m^3/kmol.s)

k_2: Forward reaction kinetic rate constant of Reaction 4.2-2 (m^3/kmol.s)

COMSOL Multiphysics expects rate constants for all reactions. Approximation to the assumption that reactions 4.2-3, 4.2-4 and 4.2-5 are instantaneous, the reaction constants k_3, k_4 and k_5 are assumed to be equal to 1000 times k_2. Table 4.8.2-A shows calculated values of forward reaction kinetic rate constants for Reactions 4.2-1 and 4.2-2 at different temperatures.

Table 4.8.2-A: Calculated forward reaction kinetic rate constants for Reactions 4.2-1 and 4.2-2 at different temperatures

T (K)	k_1 (m³/mol.s)	k_2 (m³/mol.s)
293.15	0.665	5.748
298.15	0.786	8.416
303.15	0.923	12.169
308.15	1.079	17.387
313.15	1.256	24.560
318.15	1.454	34.318
323.15	1.675	47.458
328.15	1.922	64.985
333.15	2.197	88.150

4.8.3 CO_2 Solubility in AMP Solution

The CO_2 solubility in AMP solution was estimated at different AMP concentrations and operating temperatures using the nitrous oxide analogy method [14]:

$$H_{CO_2-amine} = H_{N_2O-amine}\left(\frac{H_{CO_2-water}}{H_{N_2O-water}}\right)$$ 4.8-8

where:

$H_{CO_2-amine}$: Henry's constant of CO_2 into AMP aqueous solution (Pa.m³/mol)

$H_{N_2O-amine}$: Henry's constant of N_2O into AMP aqueous solution (Pa.m³/mol)

$H_{CO_2-water}$: Henry's constant of CO_2 into water (Pa.m³/mol)

$H_{N_2O-water}$: Henry's constant of N_2O into water (Pa.m³/mol)

The solubility of nitrous oxide in amine solution was estimated using the following equation;

$$H_{N_2O-amine} = (5.52 + 0.7C) \times 10^6 \exp\left(\frac{-2166}{T}\right)$$ 4.8-9

where:

C: AMP concentration (kmol/m³)

The solubility of nitrous oxide and carbon dioxide in water were estimated using the following equations:

$$H_{N_2O-water} = 8.5470 \times 10^6 \exp\left(\frac{-2284}{T}\right) \qquad 4.8-10$$

$$H_{CO_2-water} = 2.8249 \times 10^6 \exp\left(\frac{-2044}{T}\right) \qquad 4.8-11$$

Henry's constants of CO_2 into AMP aqueous solution ($H_{CO_2-amine}$) were calculated at different temperatures and AMP concentrations and the results are shown in Figure 4.8.3-A.
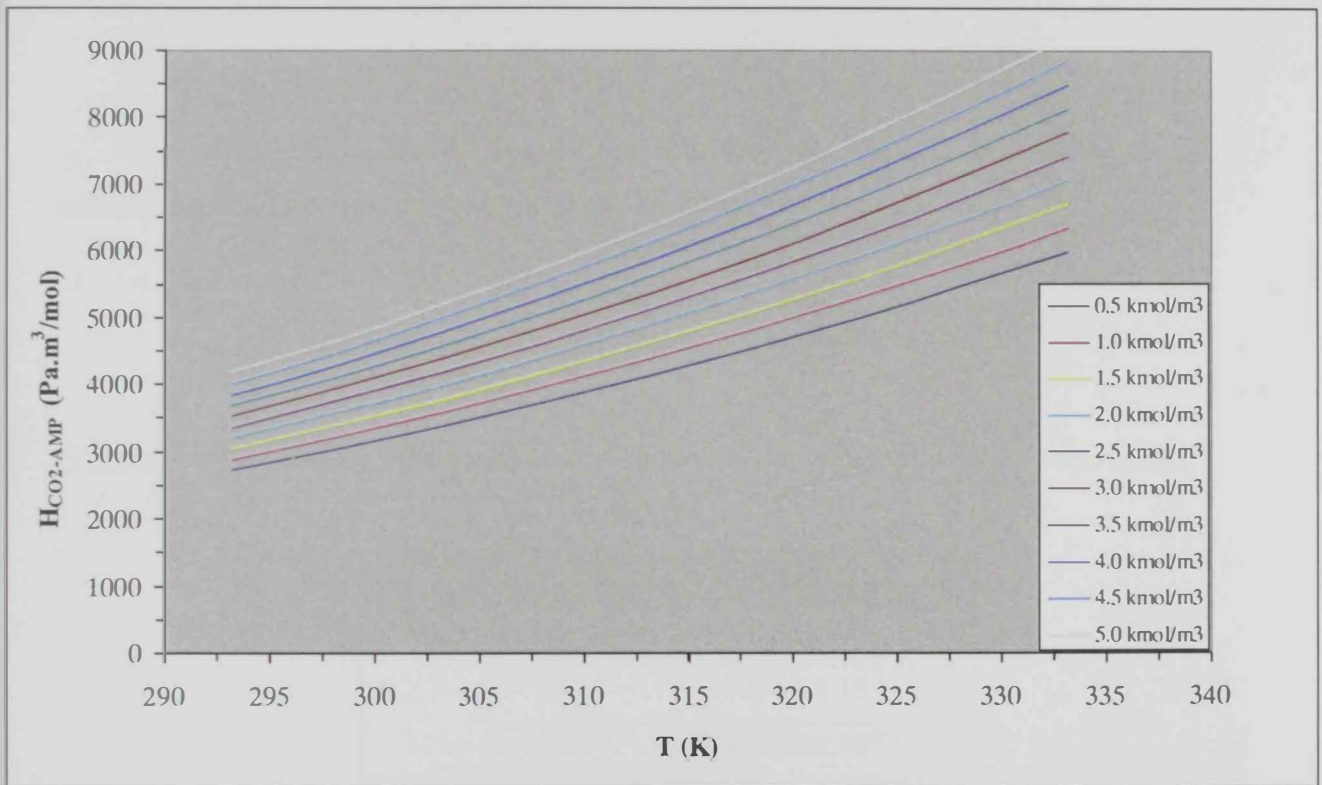

Figure 4.8.3-A: Calculated Henry's constants of CO_2 into AMP aqueous solution at different temperatures and AMP concentrations

In general as Henry's constant increases the gas solubility in liquid phase decreases. Figure 4.8.3-A shows the effect of temperature and AMP concentration on Henry's constant of CO_2 into AMP aqueous solution. Higher temperature and AMP concentration leads to higher Henry's constant and subsequently lower CO_2 solubility into AMP aqueous solution.

4.8.4 Density of AMP Solution

The density of AMP solution was estimated at different AMP concentrations and operating temperatures using the Redlich-Kister equation for the excess molar volume [20]:

$$V_{12}^E = x_1\, x_2 \sum_{i=0}^{n} A_i (x_1 - x_2)^i$$

4.8-12

where:

V_{12}^E : excess molar volume (cm^3/mol)

x_1 : AMP mole fraction

x_2 : water mole fraction

A_i: pair parameters, are assumed to be temperature dependent and can be estimated using Equation 4.8-13 (see Table 4.8.4-A);

$$A_i = a + bT + cT^2$$

4.8-13

Where a, b, c are parameters and they are available in Table 4.8.4-A.

Table 4.8.4-A: Binary parameters of the Redlich-Kister equation of the excess molar volume

A_i		AMP (1) + H_2O (2)
	a	- 6.51042
A_o	b	5.02584×10^{-3}
	c	1.08578×10^{-6}
	a	5.55560
A_1	b	-1.1325×10^{-2}

After computing A_o and A_1 using Equation 4.8-13 and Table 4.8.4-A, the excess molar volume can be estimated using Equation 4.8-12.

The molar volume of AMP solution can be calculated by

$$V_m = V_{12}^E + \sum x_i\, V_i^o$$

4.8-14

where:

V_m : Molar volume of AMP solution (cm^3/mol)

x_i : Mole fractions of species i AMP (1) or water (2)

V_i^o : Pure molar volumes of species i AMP (1) or water (2) (cm^3/mol)

The pure molar volumes (V_i^o) of AMP and water are required to find molar volume of the mixture. The densities (ρ_i^o) of pure AMP and water are calculated by;

$$\rho_i^o = a_1 + a_2\, T + a_3\, T^2 \qquad\qquad 4.8\text{-}15$$

where:

ρ_i^o : Pure densities of species i AMP (1) or water (2) (g/cm^3)

Table 4.8.4-B: Parameters of the density equation for pure fluid.

Pure Fluid	a_1	a_2	a_3
AMP	1.15632	-6.76170 x 10^{-4}	-2.67580 x 10^{-7}
H_2O	0.863559	1.21494 x 10^{-3}	-2.57080 x 10^{-6}

In order to estimate the pure molar volume of AMP and water from corresponding densities, the compound chemical molecular weight was divided by its density;

$$V_i^o = \frac{M_i}{\rho_i^o} \qquad\qquad 4.8\text{-}16$$

Finally the density of AMP solution (ρ_m) can be estimated by the following equation

$$\rho_m = \frac{\sum x_i\, M_i}{V_m} \qquad\qquad 4.8\text{-}17$$

The densities of AMP aqueous solution (ρ_m) were estimated at different temperatures and AMP concentrations and the results are shown in Figure 4.8.4-A.
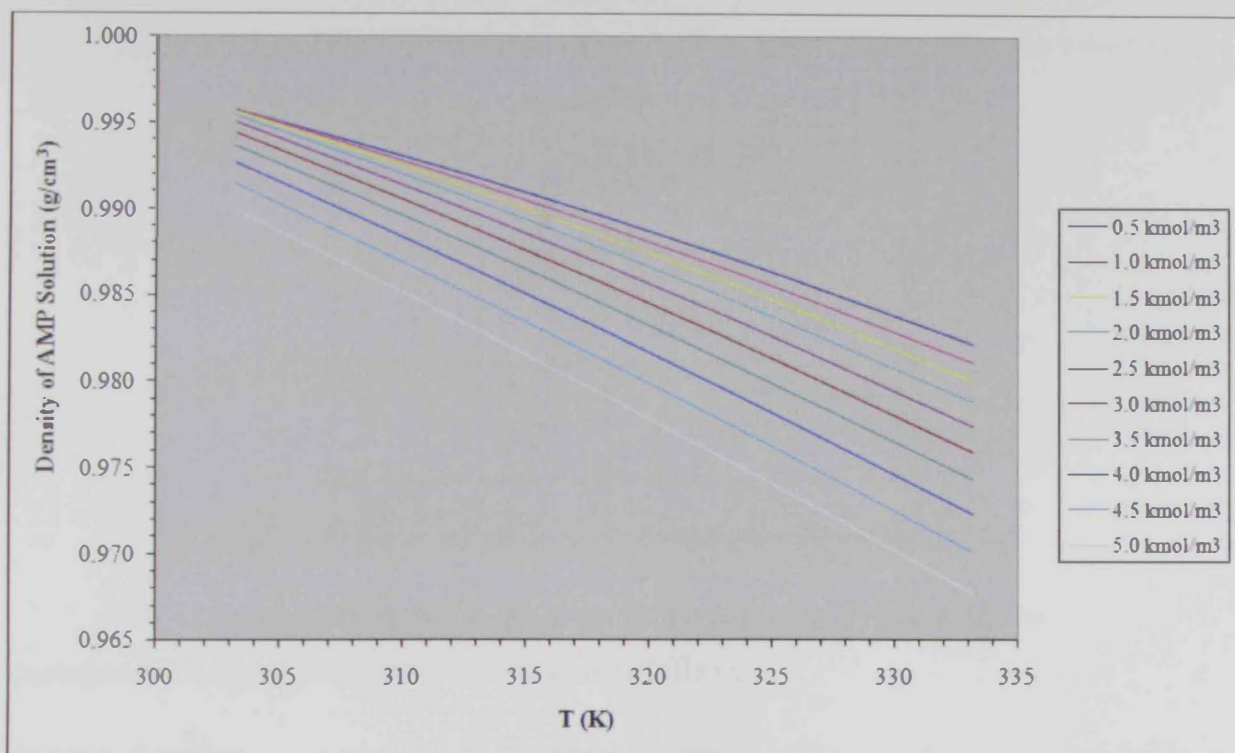
Figure 4.8.4-A: Calculated densities of AMP aqueous solution at different temperatures and AMP concentrations

4.8.5 Dynamic Viscosity of AMP Solution

The kinematic viscosity of AMP solution (v_m) was estimated at different AMP concentrations and operating temperatures using Redlich-Kister equation for the viscosity deviation [21]:

$$\delta v_{12} = x_1 \, x_2 \sum_{i=0}^{m} A_i (x_1 - x_2)^i \qquad\qquad 4.8\text{-}18$$

where A_i are pair parameters, determined by:

$$A_i = a + \frac{b}{T + c} \qquad\qquad 4.8\text{-}19$$

where a, b, c are parameters, available in Table 4.8.5-A.

Table 4.8.5-A: Binary parameters of the Redlich-Kister equation for the viscosity deviation

A_i		AMP (1) + H_2O (2)
A_o	a	4.01239
	b	2.49856×10^2
	c	$- 2.65712 \times 10^2$
A_1	a	- 2.68462
	b	0
A_2	c	0

The kinematic viscosity of the pure fluid, required to calculate the viscosity deviation as in Equation 4.8-18, is calculated as follows:

$$\ln v = a_1 + \frac{a_2}{T + a_3}$$
4.8-20

where a_i are parameters (see Table 4.8.5-B) and are determined from kinematic viscosities of pure fluids.

Table 4.8.5-B: Parameters of the kinematic viscosity equation for pure fluids

Pure Fluid	a_1	a_2	a_3
AMP	-4.36785	9.96598×10^2	-1.92984×10^2
H_2O	-3.28285	4.56029×10^2	-1.54576×10^2

The kinematic viscosity of AMP solution (v_m) can be estimated by the following equation:

$$v_m = \exp\left(\delta v_{12} + \sum_{i=1}^{n} x_i \ln v_i \right)$$
4.8-21

where v is the kinematic viscosity. The subscripts m and i represent the mixture and the i-th pure fluid, respectively.

Finally, the dynamic viscosity of AMP solution (μ_m) can be estimated using ρ_m as described in section 4.8.4:

$$\mu_m = v_m \rho_m$$
4.8-22

The dynamic viscosities of AMP aqueous solution (μ_m) were estimated at different temperatures and AMP concentrations and the results are shown in Figure 4.8.5-A.
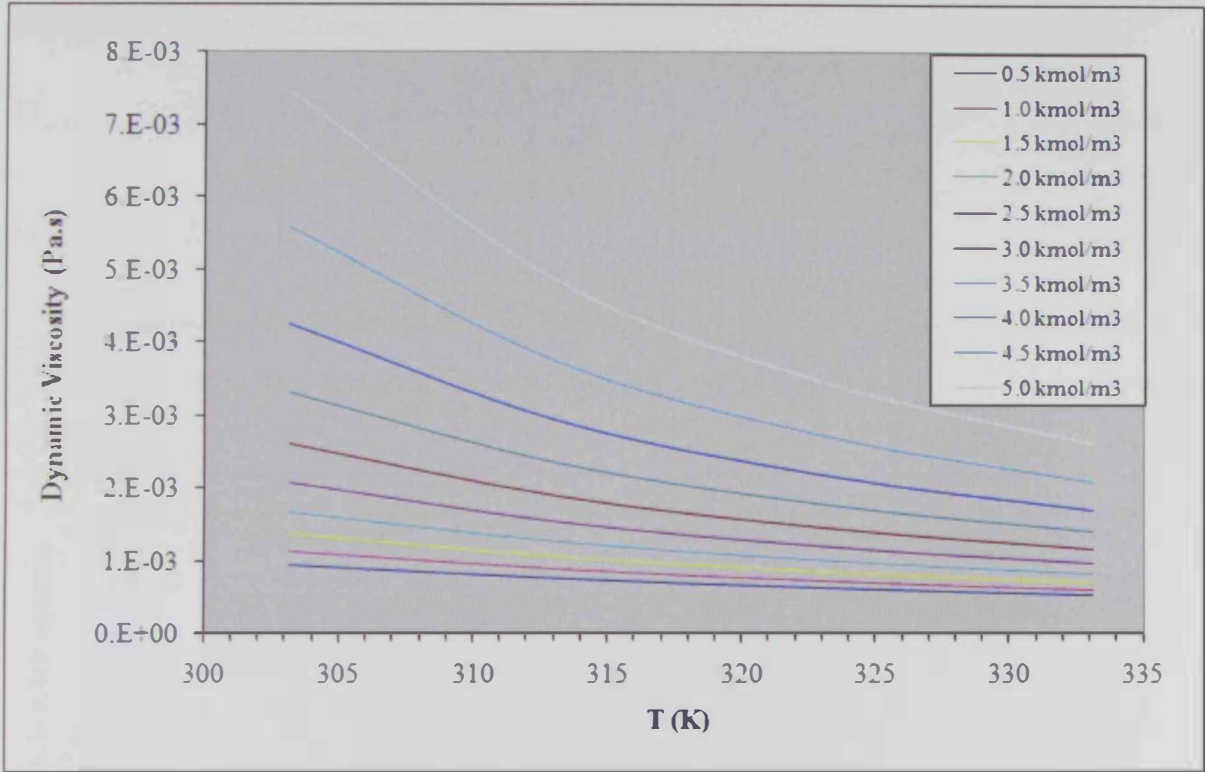

Figure 4.8.5-A: Calculated dynamic viscosities of AMP aqueous solution at different temperatures and AMP concentrations

4.8.6 CO₂ Diffusion Coefficient in AMP Solution

The CO_2 diffusion coefficient in AMP solution was estimated at different AMP concentrations and operating temperatures using the nitrous oxide analogy method [22]:

$$D_{CO_2-\text{amine}} = D_{N_2O-\text{amine}}\left(\frac{D_{CO_2-\text{water}}}{D_{N_2O-\text{water}}}\right) \qquad 4.8\text{-}23$$

where:

$D_{CO_2-\text{amine}}$: Diffusion coefficient of CO_2 into AMP aqueous solution (m^2/s)

$D_{N_2O-\text{amine}}$: Diffusion coefficient of N_2O into AMP aqueous solution (m^2/s)

$D_{CO_2-\text{water}}$: Diffusion coefficient of CO_2 into water (m^2/s)

$D_{N_2O-\text{water}}$: Diffusion coefficient of N_2O into water (m^2/s)

The diffusion coefficient of nitrous oxide in amine solution was estimated using the following equation [22]:

$$D_{N_2O-amine} = \frac{2.12 \times 10^{-14} \, T}{\mu_m^{0.82}}$$
4.8-24

The diffusion coefficient of nitrous oxide and carbon dioxide in water were estimated using the following equations [14]:

$$D_{N_2O-water} = 5.07 \times 10^{-6} \exp\left(\frac{-2371}{T}\right)$$
4.8-25

$$D_{CO_2-water} = 2.35 \times 10^{-6} \exp\left(\frac{-2119}{T}\right)$$
4.8-26

The diffusion coefficients of CO_2 into AMP aqueous solution were estimated at different temperatures and AMP concentrations and the results are shown in Figure 4.8.6-A.
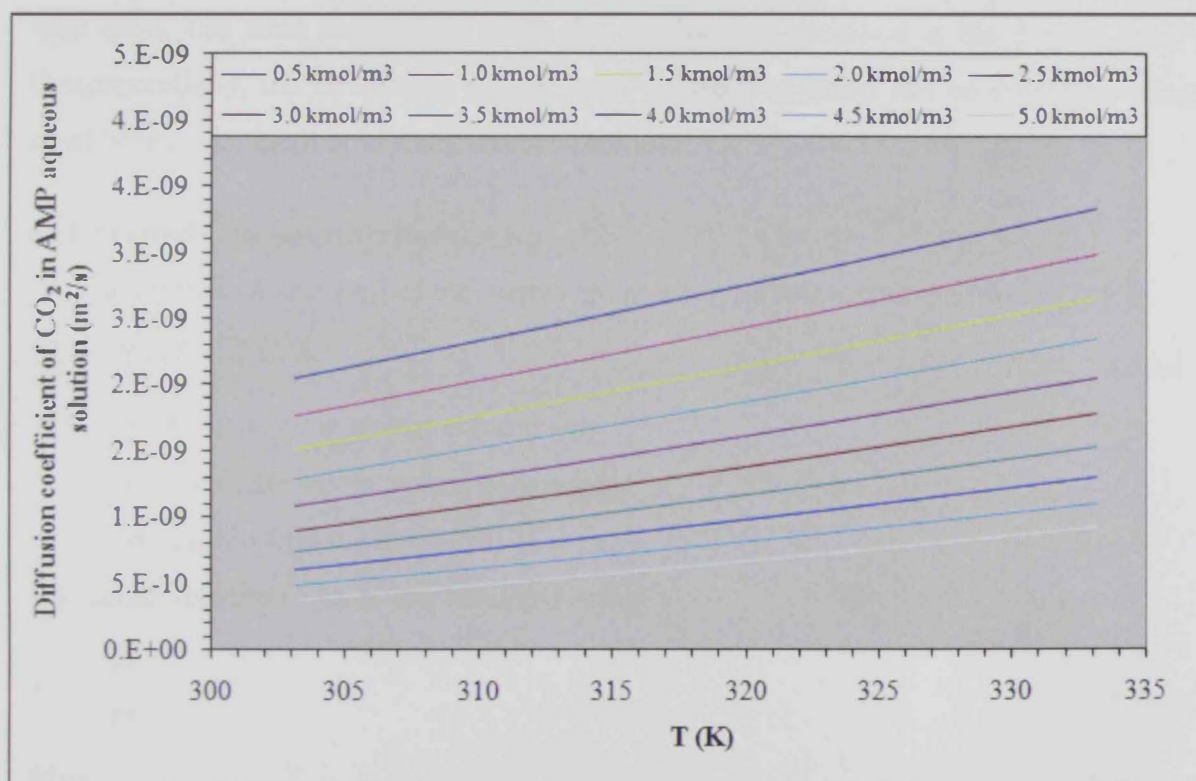

Figure 4.8.6-A: Calculated diffusion coefficients of CO_2 into AMP aqueous solution at different temperatures and AMP concentrations

It is interesting to analyze the effect of AMP concentration by observing Figures 4.8.3-A and 4.8.6-A. High concentrations of AMP higher the value of the Henry's constant (Figure 4.8.3-A) and thus decrease the solubility of CO_2 in the AMP Solution. Also, high concentrations of AMP decrease the diffusion coefficient of CO_2 in AMP solutions, making the mass diffusion process slower (Figure 4.8.6-A). Both solubility and diffusion coefficient correspond to the physical absorption. However, high

concentrations of AMP increase the chemical absorption. Therefore, the absorber design should represent a compromise between physical and chemical absorptions.

4.9 CO_2 Loading in AMP Aqueous Solution

The CO_2 loading in AMP aqueous solution (α) (mol CO_2 /mol AMP) can be calculated using the following equation [14]:

$$\alpha = \frac{c_1 + c_4 + c_6}{[AMP]_{initial}}$$ 4.9-1

The equilibrium CO_2 loading in AMP aqueous solution at the specific operating condition (CO_2 partial pressure, operating temperature and amine concentration) can be determined by solving the model and observing the change in CO_2 loading in AMP aqueous solution along with time. The time required to reach the equilibrium condition is the contact time (θ). Consequentially, the circulation rate of AMP aqueous solution can be estimated using the equilibrium CO_2 loading in AMP aqueous solution.

4.10 Wetted Column Interfacial Area

The interfacial area (A_i) of the wetted column can be calculated as follows [23]:

$$A_i = \pi (d - 2\delta) h$$ 4.10-1

h : Height of the wetted column (m)

d : Diameter of the wetted column (m)

δ : Liquid film thickness (m)

The liquid velocity (v_z) can be calculated using;

$$v_z = \frac{h}{\theta}$$ 4.10-2

Also;

$$v_z = \frac{Q_L}{Thickness\ Cross\ Section\ Area} = \frac{Q_L}{\frac{\pi}{4}(d^2 - (d - 2\delta)^2)}$$ 4.10-3

where:

Q_L : Volumetric liquid flow rate of AMP aqueous solution (m³/sec)

From Equations 4.10-2 and 4.10-3:

$$\frac{h}{\theta} = \frac{Q_L}{\frac{\pi}{4}(d^2 - (d - 2\delta)^2)}$$ 4.10-4

Therefore;

$$h = \frac{\theta\,Q_L}{\frac{\pi}{4}(d^2 - (d-2\delta)^2)} \qquad\qquad 4.10\text{-}5$$

By substituting of Equation 4.10-5 in Equation 4.10-1:

$$A_i = \pi\,(d-2\delta)\,\frac{\theta\,Q_L}{\frac{\pi}{4}(d^2 - (d-2\delta)^2)}$$

$$= 4\,\theta\,Q_L\,\frac{(d-2\delta)}{(d^2 - (d-2\delta)^2)}$$

$$= 4\,\theta\,Q_L\,\frac{(d-2\delta)}{(d^2 - (d^2 - 4d\delta + 4\delta^2))}$$

$$A_i = 4\,\theta\,Q_L\,\frac{(d-2\delta)}{(4d\delta - 4\delta^2)} \qquad\qquad 4.10\text{-}6$$

By assuming $d \ggg \delta$:

$$A_i = 4\,\theta\,Q_L\,\frac{d}{4d\delta} = \frac{\theta\,Q_L}{\delta} \qquad\qquad 4.10\text{-}7$$

Equation 4.10-7 shows the interfacial area is mainly function of contact time, volumetric flow rate of aqueous AMP solution and thickness of the falling film.

4.11 pH of AMP Aqueous solution

Estimating of AMP aqueous solution pH is essential for design and operation. Both low and high pH cause operational troubles. pH below 7 is considered corrosive media and high pH increases scale formation if AMP solution is prepared with non de-mineralized water. For this reason, it is highly recommended to use de-mineralized water to avoid scale formation. Also, the pH of lean AMP aqueous solution indicates the regeneration performance.

pH of AMP aqueous solution can be determined using following equation

$$pH = -\log\left[\frac{[H^+]}{1000}\right] \qquad\qquad 4.11\text{-}1$$

where $[H^+]$ is hydrogen concentration in mol/m^3

The pH of AMP (0.1 M) is 11.3 as per AMP material safety data sheet prepared by Caledon Laboratories Ltd [24].

CHAPTER V
RESULTS AND DISCUSSIONS

CHAPTER V
RESULTS AND DISCUSSIONS

5.1 Introduction

In this thesis the modeling and simulation of the absorption of dilute CO_2 into falling film of aqueous solutions of a sterically hindered amine, 2-amino-2-methyl-1-propanol (AMP) was carried out using COMSOL Multiphysics Version 3.3. CO_2 loading of aqueous AMP solution was estimated at different operating parameters; CO_2 partial pressure, operating temperature and amine concentration. The thickness of falling film was assumed constant and equal to 1×10^{-4} m.

5.2 Model Validation

Figure 5.2-A shows the results of calculation of CO_2 loading in AMP at same operating condition of Table 3.2.3-A: CO_2 partial pressure 9.8 kPa, AMP 1 kmol/m^3 and temperature 40°C [11].
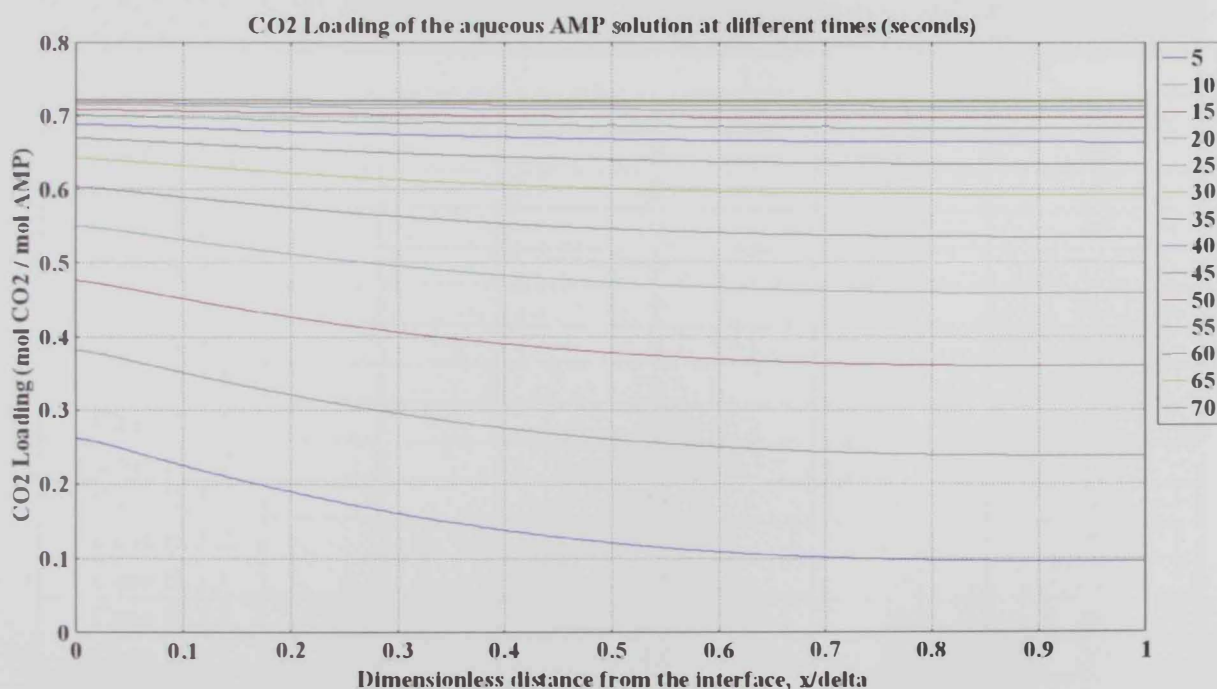

Figure 5.2-A: CO_2 loading of AMP at different times (seconds)

From Figure 5.2-A, the predicted CO_2 loading using the thesis model is 0.725, which is similar to the experimental measured value 0.755 [11]. Therefore, the modeling percentage error is 3.97 %. Moreover the model predicts meaningful trends for the effect of CO_2 partial pressure, temperature, and AMP concentration on the absorption process.

5.3 Operating Cases

The operating cases were classified in two groups: (I) Gas Turbine operating cases and (II) Boiler operating cases. Typically CO_2 content in flue gas composition is 3 vol % and 8.5 vol % for gas turbine and boiler, respectively. CO_2 content in gas turbine flue gas is lower than in boiler flue gas because of excess air utilizes for cooling. For stoichiometric combustion, the gas turbine requires approximately one-fourth of the total air it compresses. The excess air is used to cool the combustion chamber and mixes with the combustion products to reduce the gas temperature at the inlet to the first turbine stage.

Tables 5.2-A and 5.2-B shows all studied operating cases required to carry out the operating parameters optimization for gas turbine and boiler cases.

Table 5.2-A: Operating parameters of (I) gas turbine cases

Case Name	AMP Aqueous Solution Concentration		Operating Pressure	Operating Temperature
	kmol/m^3	AMP Mass %	Psig	°C
I-Case A.1.1	1	9	0	20
I-Case A.1.2	1	9	0	40
I-Case A.2.1	1	9	100	20
I-Case A.2.2	1	9	100	40
I-Case A.3.1	1	9	200	20
I-Case A.3.2	1	9	200	40
I-Case A.4.1	1	9	300	20
I-Case A.4.2	1	9	300	40
I-Case B.1.1	2	18	0.	20
I-Case B.1.2	2	18	0	40
I-Case B.2.1	2	18	100	20
I-Case B.2.2	2	18	100	40
I-Case B.3.1	2	18	200	20
I-Case B.3.2	2	18	200	40
I-Case B.4.1	2	18	300	20
I-Case B.4.2	2	18	300	40
I-Case C.1.1	3	27	0	20
I-Case C.1.2	3	27	0	40
I-Case C.2.1	3	27	100	20
I-Case C.2.2	3	27	100	40
I-Case C.3.1	3	27	200	20
I-Case C.3.2	3	27	200	40
I-Case C.4.1	3	27	300	20
I-Case C.4.2	3	27	300	40

Table 5.2-B: Operating parameters of (II) boiler cases

Case Name	AMP Aqueous Solution Concentration		Operating Pressure	Operating Temperature
	kmol/m^3	AMP Mass %	Psig	°C
II-Case A.1.1	1	9	0	20
II-Case A.1.2	1	9	0	40
II-Case A.2.1	1	9	100	20
II-Case A.2.2	1	9	100	40
II-Case B.1.1	2	18	0	20
II-Case B.1.2	2	18	0	40
II-Case B.2.1	2	18	100	20
II-Case B.2.2	2	18	100	40
II-Case C.1.1	3	27	0	20
II-Case C.1.2	3	27	0	40
II-Case C.2.1	3	27	100	20
II-Case C.2.2	3	27	100	40

5.4 Cases Results

The simulation of modeling focused on the following results:

1. CO_2 Loading in aqueous AMP solution

2. Required contact time to reach equilibrium

3. pH of rich AMP aqueous solution

4. Total required interfacial area /circulated AMP aqueous solution

Tables 5.3-A and 5.3-B summarize the results of (I) Gas Turbine cases and (II) Boiler cases.

Table 5.3-A: Summary table of (I) gas turbine cases results

Case Name	Required Contact time to reach equilibrium	Total required interfacial area / Circulated AMP Aqueous Solution	CO$_2$ Loading in AMP Aqueous Solution	pH of Rich AMP Aqueous Solution
	Seconds	s/m	Mol CO$_2$ / Mol AMP	
I-Case A.1.1	200	2000000	0.750	9.30
I-Case A.1.2	140	1400000	0.525	9.16
I-Case A.2.1	60	600000	0.950	8.50
I-Case A.2.2	50	500000	0.850	8.54
I-Case A.3.1	40	400000	0.970	8.21
I-Case A.3.2	40	400000	0.913	8.28
I-Case A.4.1	30	300000	1.000	8.10
I-Case A.4.2	25	250000	0.950	8.14
I-Case B.1.1	300	3000000	0.625	9.53
I-Case B.1.2	200	2000000	0.400	9.38
I-Case B.2.1	100	1000000	0.900	8.80
I-Case B.2.2	60	600000	0.733	8.80
I-Case B.3.1	60	600000	0.950	8.55
I-Case B.3.2	50	500000	0.825	8.58
I-Case B.4.1	55	550000	0.967	8.40
I-Case B.4.2	45	450000	0.875	8.45
I-Case C.1.1	480	4800000	0.550	9.65
I-Case C.1.2	260	2600000	0.333	9.50
I-Case C.2.1	140	1400000	0.860	9.00
I-Case C.2.2	80	800000	0.650	8.96
I-Case C.3.1	100	1000000	0.917	8.75
I-Case C.3.2	70	700000	0.760	8.77
I-Case C.4.1	100	1000000	0.940	8.60
I-Case C.4.2	60	600000	0.813	8.63

Table 5.3-B: Summary table of (II) boiler cases results

Case Name	Required Contact time to reach equilibrium	Total required interfacial area / Circulated AMP Aqueous Solution	CO_2 Loading in AMP Aqueous Solution	pH of Rich AMP Aqueous solution
	Seconds	s/m	Mol CO_2 / Mol AMP	
II-Case A.1.1	90	900000	0.880	8.900
II-Case A.1.2	70	700000	0.700	8.875
II-Case A.2.1	30	300000	1.000	8.042
II-Case A.2.2	22	220000	0.950	8.104
II-Case B.1.1	160	1600000	0.79	9.18
II-Case B.1.2	110	1100000	0.567	9.11
II-Case B.2.1	55	550000	0.967	8.375
II-Case B.2.2	34	340000	0.875	8.417
II-Case C.1.1	240	2400000	0.717	9.333
II-Case C.1.2	140	1400000	0.483	9.250
II-Case C.2.1	80	800000	0.945	8.58
II-Case C.2.2	60	600000	0.817	8.60

5.5 Effect of the Key Parameters

The results of Tables 5.2-A, 5.2-B, 5.3-A and 5.3-B show that:

➤ The CO_2 loading in AMP aqueous solution approached one for some cases and below 0.5 for other cases.

➤ High operating pressure increases CO_2 loading as it increases the partial pressure of CO_2 and consequently increases the equilibrium CO_2 solubility concentration at the interface. This can be observed by comparing cases I.A.1.1, I.A.2.1, I.A.3.1, and I.A.4.1, for example.

➤ Low operating temperature decreases Henry's constant of CO_2 in AMP aqueous solution, increasing the equilibrium CO_2 solubility concentration at the interface. However, low operating temperature decreases the speed of reaction. The overall effect of lowering the temperature is to enhance CO_2 loading. This can be observed by comparing cases I.A.1.1 with I.A.1.2, cases I.A.2.1 with I.A.2.2, etc.

➤ Low AMP aqueous concentration increases CO_2 loading as it decreases the viscosity thereby increasing the diffusion coefficient. This can be observed by comparing cases I.A.1.1, I.B.1.1, and I.C.1.1, for example.

➤ The compression requirement for gas turbine flue gas is found to be higher than for the boiler flue gas because CO_2 partial pressure is low in case of gas turbine.

➤ The pH of rich AMP aqueous solution at maximum CO_2 loading was 8. Having the pH of rich amine larger than 7 reduces the risk of high corrosion environment.

➤ The required contact time to reach equilibrium decreases with temperature increases because of faster speeds of reaction. This can be observed by comparing cases I.A.1.1 with I.A.1.2, cases I.A.2.1 with I.A.2.2, etc.

CHAPTER VI

DESIGN ESTIMATION OF STRUCTURED PACKED ABSORBER
COLUMN FOR GAS TURBINE AND BOILER CASE STUDIES

CHAPTER VI

DESIGN ESTIMATION OF STRUCTURED PACKED ABSORBER COLUMN FOR GAS TURBINE AND BOILER CASE STUDIES

6.1 Introduction

The results from chapter 5 were utilized to estimate the lower bound to the size of absorbers for the gas turbine and boiler case studies for 100 MMSCFD total flue gas flow rate; which is in the range of two to three gas turbine units in simultaneous operation. It is recommended to avoid excessive cooling of flue gas in order to the required amount of cooling water. Moreover, the higher temperature decreases the contact time to reach equilibrium condition. Also, it is recommended to minimize the operating pressure of absorber column to avoid large compressor requirement that results from compressing flue gas from atmospheric pressure. In general using higher concentration of AMP solution reduces the circulated AMP solution flow rate. However, higher concentration decreases CO_2 loading of AMP solution.

6.2 Design Estimation of Structural Packed Absorber for Gas Turbine Case Study

I-Case B.2.2 was selected to be the most suitable case for gas turbine. Only 100 psig is required to compress the flue gas down stream the direct cooler. 40°C temperature is required to run the absorption unit which will reduce the required amount of cooling water of flue gas.

6.2.1 Estimation of Circulated AMP Aqueous Solution

An estimate of minimum AMP flow rate can be obtained from equilibrium CO_2 loading [25]. For I-Case B.2.2 the AMP CO_2 loading is 0.733 mol-CO_2/mol-AMP. The molar CO_2 flow rate calculated as:

CO_2 Molar Flow = CO_2 Mole Fraction * Total Flue Gas Molar Flow   6.2-1

$= 0.03 * 100$ MMSCFD $= 0.03 * 119786500$ mol/day $= 3593595$ mol/day

CO_2 Mass Flow = CO_2 Molar Flow / MW_{CO2} 6.2-2

$= 3593595$ mol/day / $44 = 158.118$ M.tonnes/day.

AMP Pure Molar flow (Minimum) = CO_2 molar flow / CO_2 Loading   6.2-3

$= 3593595$ mol/day / 0.733 mol-CO_2/mol-AMP $= 4902585$ mol/day

AMP Solution Molar flow (Minimum) = AMP Pure Molar flow (Minimum) / AMP Mole Fraction   6.2-4

$= 4902585$ mol/day / $0.0425 = 115363142$ mol/day

AMP Solution Mass flow (Minimum) = AMP Solution Molar flow (Minimum) * MW_{AMP}
Solution   6.2-5

$$= 115363142 \text{ mol/day} * 21.042 \text{ g/mol} = 2427515677 \text{ g/day}$$

AMP Solution Volumetric flow (Minimum) = AMP Solution Mass flow (Minimum) / average AMP Solution density   6.2-6

$$= 2427515677 \text{ g/day} * 0.9903 \text{ g/mL} = 2.837 \times 10^{-02} \text{ m}^3 / \text{s}$$

6.2.2 Estimation of Total Volume of Structured Packed Column Absorber

The channels formed by the structured packing elements are presumed to pass liquid and vapor in counter flow contacting. Since the geometry is well-defined and the packing surface area is known precisely, it has been found possible to model the mass transfer process using wetted wall theory. This idea was adopted by many investigators in the study of structured packed columns [26]. Structural packing materials are produced of metal, plastic, ceramics, and carbon. Structural packing materials are produced of metal, plastics and ceramics. The required height of structural packed column is lower than random packed column. Also, the pressure drop across structural packed column is lower than random packed column [27].

Ceramic structural packing was selected due to its high corrosion resistance. Although it can sustain higher temperatures than metal, it is not recommended to use it if there is potential for thermal shocking. So, this idea should clear appear in startup and shutdown policies to avoid damaging of column internals. Among the groups of ceramic structural packing 250Y model was selected. The wave angle and specific surface area of 250Y are 45° and $250\text{m}^2/\text{m}^3$, respectively [28]. The total minimum interfacial area required can be calculated using the result of 1-Case B.2.2. This is a lower bound to the actual interfacial area for packed column because it is calculated under the assumption that all the packing surface area is available for mass transfer. However, a part of the packing surface area may not be wet and, even if wet, it could be at a stagnant location that does not participate of the mass transfer process. Close to the flooding condition, the wetted column interfacial area and the surface area of packing are similar [29].

Total interfacial area required = $2.837 \times 10^{-02} \text{ m}^3/\text{s} * 600000\text{s/m} = 17022\text{m}^2$

Volume of structured packed column (minimum) = Total interfacial area / specific surface area of structural packing material   6.2-7

$$= 17022\text{m}^2 / 250\text{m}^2/\text{m}^3 = 68.088 \text{ m}^3$$

6.2.3 Estimation of Structured Packed Column Absorber Diameter and Height

The diameter of any type of column depends on the flooding condition as well as liquid entrainment. Fair and Bravo correlated flooding data for Mellapak 250Y packing. Their correlation shown in Figure 6.2.3-A. Their correlation uses a flooding region that is characterized by a rapid increase in pressure drop with simultaneous loss of separation efficiency [28]. This is a lower bound to the actual diameter because it is calculated at the flooding condition with ignoring the effects of foaming.

$$\text{Flow Parameter} = \frac{M_l}{M_g}\sqrt{\frac{\rho_g}{\rho_l}} \qquad\qquad 6.2\text{-}8$$

where:

M_l : AMP liquid mass flow rate

M_g : Flue gas mass flow rate

ρ_l : AMP liquid density

ρ_g : Flue gas density

$$\text{Flow Parameter} = \frac{2427515677 \text{ g/day}}{3354022000 \text{ g/day}}\sqrt{\frac{0.531\,\text{lb/ft}^3}{61.824\,\text{lb/ft}^3}} = 0.067$$
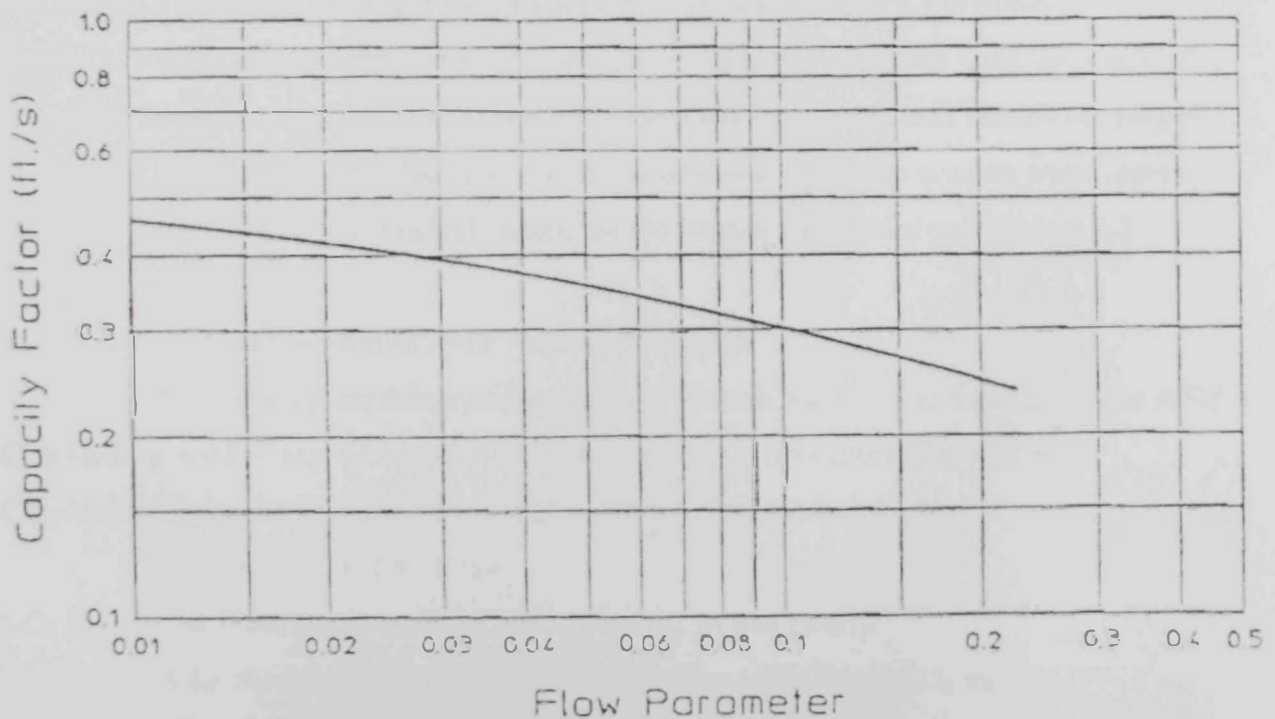
Figure 6.2.3-A: Flooding capacity of Mellapak 250Y packing [28]

54

From Figure 6.2.3-A, the capacity factor is 0.333 ft/s.

$$\text{Capacity Factor} = \frac{G_p}{\sqrt{\rho_g(\rho_l - \rho_g)}} \qquad 6.2\text{-}9$$

where:

G_p : Tower vapor loading (lb/ft^2 sec)

Capacity Factor in unit of ft/s

ρ_l and ρ_g in unit of lb/ft^3

$$G_p = 0.333 \text{ ft/s} * \sqrt{0.531 \text{ lb/ft}^3 * (61.824 \text{ lb/ft} - 0.531 \text{ lb/ft}^3)} = 1.900 \text{ lb/ft}^2 \text{ sec}$$

Column cross section area = M_g / G_P 6.2-10

$$= 85.583 \text{ lb/sec} / 1.900 \text{ lb/ft}^2 \text{ sec} = 4.185 \text{ m}^2$$

$$\text{Column cross section diameter} = \sqrt{\frac{4 * \text{Area}}{\pi}}$$

$$= \sqrt{\frac{4 * 4.185}{\pi}} = 2.3 \, m \qquad 6.2\text{-}11$$

Column height = Column Volume / Cross Section Area

$$= 68.088\text{m}^3 / 4.185 \text{ m}^2 = 16.3 \text{ m} \qquad 6.2\text{-}12$$

6.3 Design Estimation of Structured Packed Absorber for Boiler Case Study

II-Case B.1.2 was selected to be the most suitable case for boiler. No need for compressor and 40°C temperature is required to run the absorption unit which will reduce the required amount of cooling water of flue gas. As in the previous case, the column sizes represent estimated lower bounds to the actual values, for the reasons mentioned in Section 6.2.2.

6.3.1 Estimation of Circulated AMP Aqueous Solution

This section uses a procedure similar to that of section 6.2.1. For II-Case B.1.2 the AMP CO_2 loading is 0.567 mol-CO_2/mol-AMP. The molar CO_2 flow rate calculated as:

CO_2 Molar Flow = 0.085 * 100 MMSCFD = 0.085 * 119786500 mol/day

$$= 10181853 \text{ mol/day}$$

CO_2 Mass Flow = 10181853 mol/day / 44 = 448.002 M.tonnes/day.

AMP Pure Molar flow (minimum) = 10181853 mol/day / 0.567 mol-CO_2/mol-AMP

$$= 17957412 \text{ mol/day}$$

AMP Solution Molar flow (minimum) = 17957412 mol/day / 0.0425 = 422557351 mol/day

AMP Solution Mass flow (minimum) = 422557351 mol/day * 21.042 g/mol

$$= 8891614594 \text{ g/day}$$

AMP Solution Volumetric flow (minimum) = 8891614594 g/day * 0.9903 g/mL = 1.039 x $10^{-01} \text{ m}^3 / \text{s}$

6.3.2 Estimation of Total Volume of Structured Packed Column Absorber

This section uses a procedure similar to that of section 6.2.2 and the same packing material (250Y).

Total required interfacial area can be calculated using the result of II-Case B.1.2:

Total required interfacial area = 1.039 x 10^{-01} m^3/s * 1100000 s/m = 114312 m^2

Volume of structural packed column = 114312 m^2 / 250 m^2/m^3 = 457 m^3

6.3.3 Estimation of Structured Packed Column Absorber Diameter and Height

This section uses a procedure similar to that of section 6.2.3.

$$\text{Flow Parameter} = \frac{8891614594 \text{ g/day}}{3354022000 \text{ g/day}} \sqrt{\frac{0.068 \text{ lb/ft}^3}{61.824 \text{ lb/ft}^3}} = 0.088$$

From Figure 6.2.3-A, the capacity factor is 0.31 ft/s.

$$G_p = 0.31 \text{ ft/s} * \sqrt{0.068 \text{ lb/ft}^3 * (61.824 \text{ lb/ft} - 0.068 \text{ lb/ft}^3)} = 0.635 \text{ lb/ft}^2 \text{ sec}$$

Column cross section area = 85.583 lb/sec / 0.635 lb/ft^2 sec = 12.511 m^2

Column height = Column Volume / Cross section area = 457 m^3 / 12.511 m^2 = 36.5 m

6.4 Summary of Results

The summary of the results of this chapter are shown in Table 6.4-A.

Table 6.4-A: Summary of results for structured absorber columns of gas turbine and boiler case studies

Parameters	Gas Turbine	Boiler
CO_2 mole % in Flue Gas	3	8.5
Operating Pressure (psig)	100	0
Operating Temperature	40	40
AMP Solution Concentration wt %	18	18
CO_2 Mass Flow (M.ton/day)	158	448
Minimum Circulated AMP Solution Flow (USGPM)	450	1647
Column Type	Ceramic Structural Packing	Ceramic Structural Packing
Column Model	250 Y	250 Y
Column Diameter (m) (lower bound)	2.3	4
Column height (m) (lower bound)	16.3	36.5

The results of column sizing diameter and height could not be found in the open literature for similar operating condition. Therefore, it is not possible to compare the results of this chapter with literature data.

CHAPTER VII
CONCLUSIONS AND SUGGESTIONS FOR FUTURE WORK

CHAPTER VII

CONCLUSIONS AND SUGGESTIONS FOR FUTURE WORK

In this thesis the modeling and simulation of the absorption of dilute CO_2 into falling film of aqueous solutions of a sterically hindered amine, 2-amino-2-methyl-1-propanol (AMP) was carried out using COMSOL Multiphysics Version 3.3. The operating cases were divided in two groups: (I) gas turbine operating cases (CO_2 3 mol %) and (II) boiler operating cases (CO_2 8.5 mol %). The key operating parameters for the studied cases are CO_2 partial pressure, operating temperature, and amine aqueous solution concentration. The simulation of modeling focused on the following:

1. CO_2 Loading in aqueous AMP solution
2. Required contact time to reach equilibrium
3. pH of rich AMP aqueous solution
4. Total required interfacial area /circulated AMP aqueous solution

The modeling was validated by solving the modeling under the specific experimental operating condition and comparing the predicted CO_2 loading with experimental results. The percentage error between the model and experimental information was 3.97 %. The CO_2 loading in AMP aqueous solution approached one for some cases and below 0.5 for other cases. High operating pressure, low operating temperature and low AMP aqueous concentration enhance CO_2 loading. The compression requirement for gas turbine flue gas was found to be higher than for boiler flue gas. The pH of rich AMP aqueous solution at maximum CO_2 loading was 8. The required contact time to reach equilibrium decreases with temperature increases. Finally, the results were utilized to estimate the size of structured packed column absorber for 100 MMSCFD total flue gas flow rate.

The main suggestion for future work is to repeat the study using aqueous of mixture of AMP (sterically hindered amine) with primary or/and secondary amines. This mixture could enhance CO_2 loading with suitable operating condition. Also, the presence of oxygen in CO_2 streams can cause severe impact in pipeline integrity and plugging of reservoir pores formation. For this reason, it is recommended to study solubility of oxygen in AMP aqueous solutions. The maximum oxygen in the injected CO_2 is 100 ppmv as mentioned in Dakota Gasification Project's CO_2 Specification for EOR [30]. Another suggestion is to study absorption at temperatures higher than 40°C. A final suggestion is to carryout experimental work for more complete model validation.

References

1. Thiyagarajan, A., "Air Pollution and Respiratory Illness," Proceedings of the Third International Conference on Environment and Health, (December-2003): 588 – 596.

2. Abu Dhabi Environment Agency Website (http://www.soe.ae).

3. Wong, S. and Bioletti, R., "Carbon Dioxide Separation Technologies," Alberta Research Council (ARC) (2002).

4. Chakravarti, S., Gupta, A., and Hunek, B., "Advanced Technology for the Capture of Carbon Dioxide from Flue Gases", First National Conference on Carbon Sequestration, Washington, May 15-17, 2001.

5. Chapel, D.G., Mariz, C.L., and Ernest, J., "Recovery of CO_2 from Flue Gases: Commercial Trends," Canadian Society of Chemical Engineers (1999).

6. Sakwattanapong, R., Aroonwilas, A., and Veawab, A., "Behavior of Reboiler Heat Duty for CO_2 Capture Plants Using Regenerable Single and Blended Alkanolamines," Ind. Eng. Chem. Res. 44, No. 12 (2005): 4465-4473.

7. Kundu, M. and Bandyopadhyay (S.S.), "Solubility of CO_2 in Water + Diethanolamine + 2-Amino-2-methyl-1-propanol," Journal of Chemical Engineering Data 51 (2006): 398-405.

8. Murrieta-Guevara, F., Rebolledo-Libreros, M.E., Romero-Martinez, A., and Trejo, A., "Solubility of CO_2 in aqueous mixtures of diethanolamine with 2-methyldiethanolamine and 2-amino-2-methyl-1-propanol," Fluid Phase Equilibria 150–151 (1998): 721–729.

9. Veawab, A., Tontiwachwuthikul, P., and Bhole, S.D., "Studies of Corrosion and Corrosion Control in a CO_2-2-Amino-2-methyl-1-propanol (AMP) Environment," Ind. Eng. Chem. Res 36, No.1, (1997): 264-269.

10. Pei, Z., Yao, S., Jianwen, W., Wei, Z., and Qing, Y., "Regeneration of 2-amino-2-methyl-1-propanol used for carbon dioxide absorption" Journal of Environmental Sciences 20, (2008): 39–44.

11. Mimura, T., Yagi, Y., Takashina, T., Yoshiyama, R., and Honda, A., "Evaluation of Alkanolamine Chemical Absorbents for CO_2 from Vapor-Liquid Equilibrium Measurements" Journal of Japan Petroleum Institute 31 (2005): 237–242.

12. Hasib-ur-Rahman, M., Siaj, M., and Larachi, F., "Ionic liquids for CO2 capture – Development and progress" Chemical Engineering and Processing 49 (2010): 313-322.

13. Mofarahi, M., Khojasteh, Y., Khaledi, H., and Farahnak, A., "Design of CO_2 absorption plant for recovery of CO_2 from flue gases of gas turbine" Energy 33 (2008): 1311– 1319.

14. Zhang, P., Shi, Y., and Wei, J.W., "Kinetics region and model for mass transfer in carbon dioxide absorption into aqueous solution of 2-amino-2-methyl-1-propanol," Separation and Purification Technology 56, (2007): 340–347.

15. Silva, E.F.D. and Svendsen, H.F., "Computational chemistry study of reactions, equilibrium and kinetics of chemical CO_2 absorption" International Journal of Greenhouse Gas Control (2007): 151-157.

16. Mandal, B. P., Biswas, A. K., and Bandyopadhyay, S.S., "Absorption of carbon dioxide into aqueous blends of 2-amino-2-methyl-1-propanol and diethanolamine," Chemical Engineering Science 58, (2003): 4137 – 4144.

17. Rebolledo-Libreros, M.E. and Trejo, A., "Gas solubility of CO_2 in aqueous solutions of N-methyldiethanolamine and diethanolamine with 2-amino-2-methyl-1-propanol," Fluid Phase Equilibria 218, (2004): 261–267.

18. COMSOL Chemical Reaction Engineering, Module Library, Absorption in a Falling Film, Version 3.3, 328-339 (2006).

19. Bird, R.B., Stewart, W.E., and Lightfoot, E.N., *Transport phenomena*, 2nd ed., John Wiley & Sons, New York, 2002.

20. Hsu, C.H. and Li, M.H., "Densities of Aqueous Blended Amines," J. Chem. Eng. Data 42, No.3 (1997): 502-507.

21. Hsu, C.H. and Li, M.H., "Viscosity of Aqueous Blended Amines," J. Chem. Eng. Data 42, No.4 (1997): 714-720.

22. Saha, A.K., Bandyopadhyay, S.S., and Biswas, A.K., "Solubility and diffusivity of nitrous oxide and carbon dioxide in aqueous solutions of 2-amino-2-methyl-1-propanol," J. Chem. Eng. Data 38, No.1 (1993): 78-82.

23. Crasue, J.C. and Nieuwoudt, I., "Mass Transfer in a Short Wetted Column. 1. Pure Components" Ind. Eng. Chem. Res. 38, No.12 (1999): 4928-4932.

24. Material safety data sheet (MSDS) of 2-amin-2-methyl-1-propanol (AMP), product code # 0880-5, October 2009.

25. Manning, F.S. and Thompson, R.E., *Oilfield Processing of Petroleum* 1, Pennwell Books, Oklahoma, 1991.

26. Wang, G.Q., Yuan, X.G., and Yu, K.T., "Review of Mass-Transfer Correlations for Packed Columns" Ind. Eng. Chem. Res. 44, No.23 (2005): 8715-8729.

27. Sinnott, R.K., *Chemical Engineering Design* 6, Fourth ed., Elseiver Butterworth-Heinemann, New York, 2005.

28. Strigle, R.F., *Packed Tower Design and Applications*, Second ed., Gulf Publishing Company, Houston, 1994.

29. Rocha, J.A., Bravo, J.L., and Fair, J.R., "Distillation Columns Containing Structured Packings: A Comprehensive Model for Their Performance. 2. Mass-Transfer Model" Ind. Eng. Chem. Res. 35, No. 5 (1996): 1660 – 1667.

30. Ramezan, M. and Skone, T.J., "Final Project Report Carbon Dioxide Capture from Existing Coal-Fired Power Plants" Research and Development Solutions (2007): DOE/NETL-401/110907.

APPENDIX A: OPERATING CASES (I) OF GAS TURBINE

This appendix displays the results for gas turbine cases. The code names are defined in Table 5.2-A.

I- Case A.1.1

CO2 Loading of the aqueous AMP solution at different times (seconds)

pH of Rich AMP Aqueous solution at different times (seconds)

I- Case A.1.2

CO2 Loading of the aqueous AMP solution at different times (seconds)

Y-axis: CO2 Loading (mol CO2 / mol AMP)
X-axis: Dimensionless distance from the interface, x/delta

Legend: 0, 10, 20, 30, 40, 50, 60, 70, 80, 90, 100, 110, 120, 130, 140

pH of Rich AMP aqueous solution at different times (seconds)

Y-axis: pH
X-axis: Dimensionless distance from the interface, x/delta

Legend: 10, 20, 30, 40, 50, 60, 70, 80, 90, 100, 110, 120, 130, 140

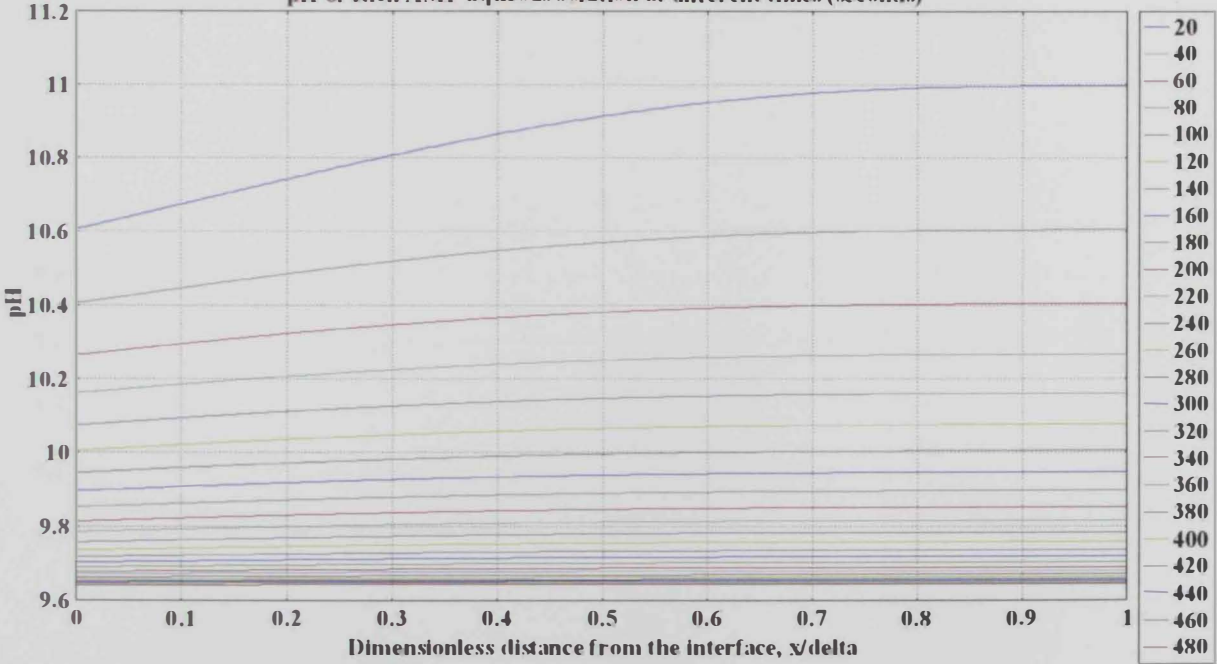# I- Case A.2.1

CO2 Loading of the aqueous AMP solution at different times (seconds)

pH of Rich AMP aqueous solution at different times (seconds)

I- Case A.2.2

CO2 Loading of the aqueous AMP solution at different times (seconds)

Y-axis: CO2 Loading (mol CO2 / mol AMP)

X-axis: Dimensionless distance from the inter ace, x/delta

Legend: 10, 20, 30, 40, 50

pH of Rich AMP aqueous solution at different times (seconds)

Y-axis: pH

X-axis: Dimensionless distance from the inter ace, x/delta
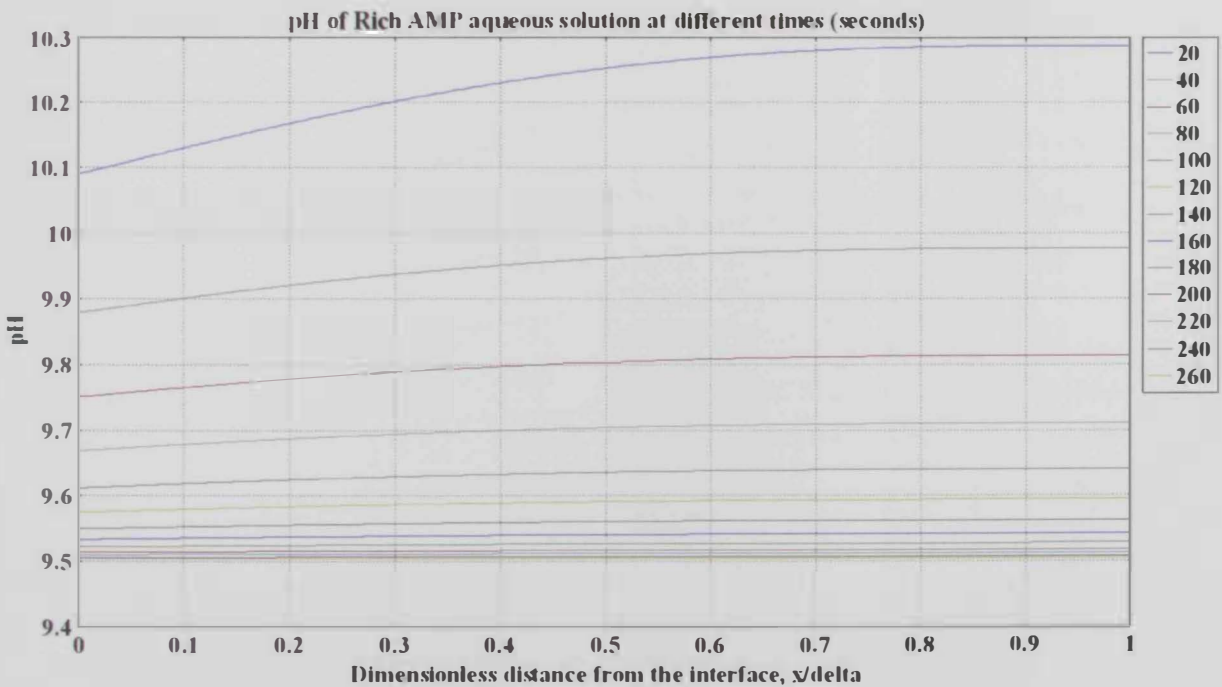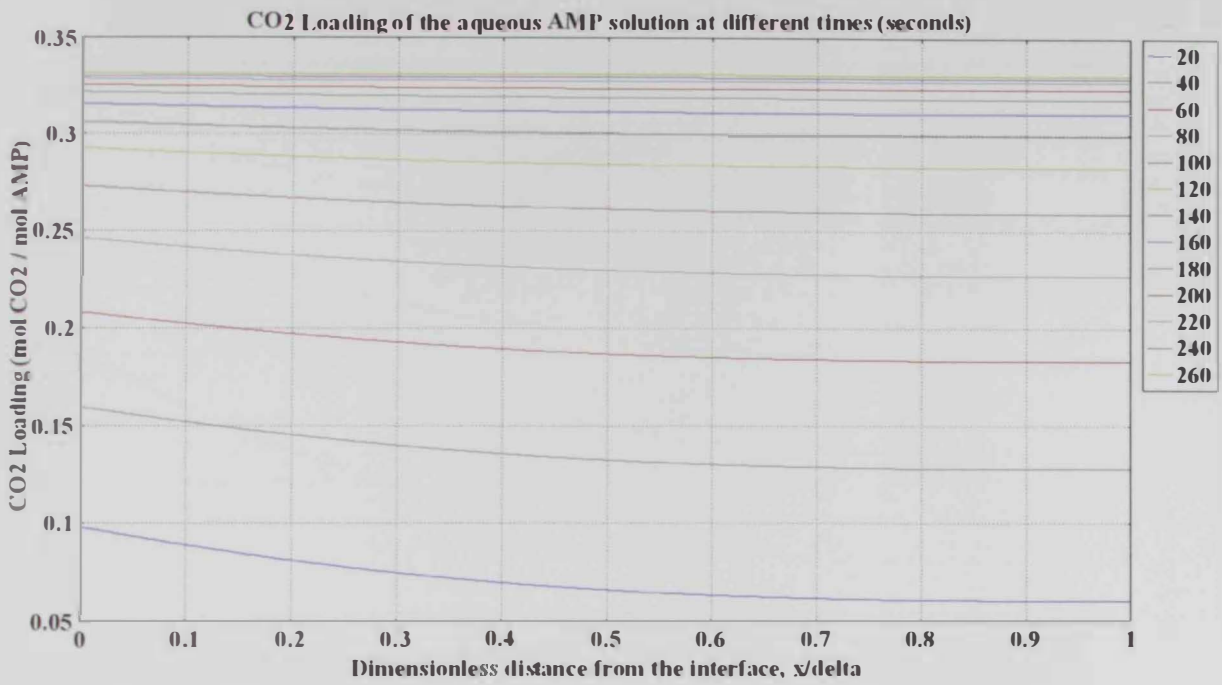
Legend: 10, 20, 30, 40, 50

I- Case A.3.1

CO2 Loading of the aqueous AMP solution at different times (seconds)

pH of Rich AMP aqueous solution at different times (seconds)

I- Case A.3.2

CO2 Loading of the aqueous AMP solution at different times (seconds)
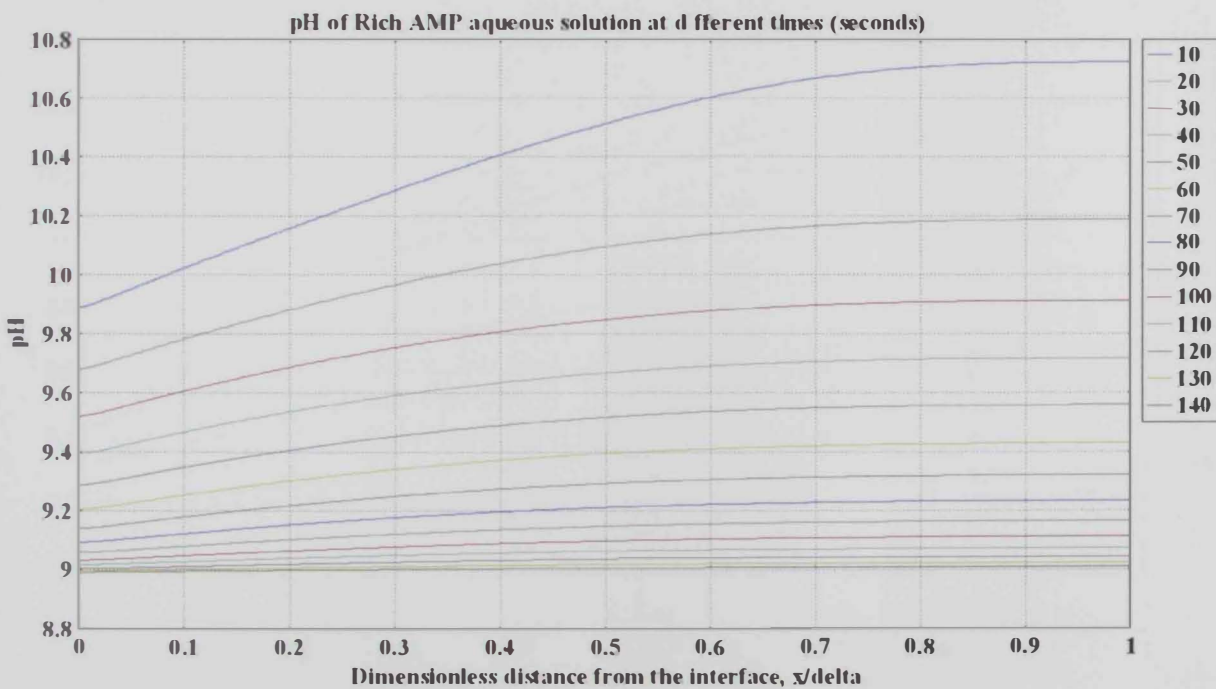

pH of Rich AMP aqueous solution at different times (seconds)

I- Case A.4.1

CO2 Loading of the aqueous AMP solution at different times (seconds)

pH of Rich AMP aqueous solution at different times (seconds)

I- Case A.4.2

CO2 Loading of the aqueous AMP solution at different times (seconds)
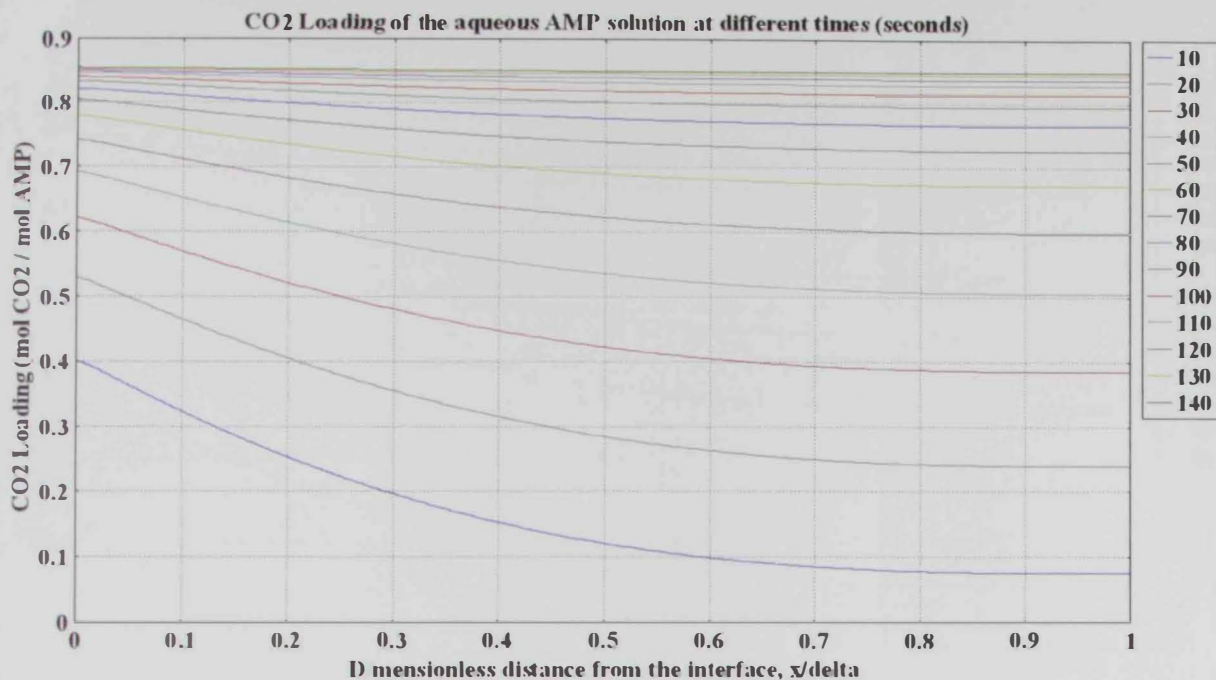

pH of Rich AMP aqueous solution at different times (seconds)

I- Case B.1.1

CO2 Loading of the aqueous AMP solution at different times (seconds)

pH of Rich AMP aqueous solution at different times (seconds)

I- Case B.1.2

CO2 Loading of the aqueous AMP solution at different times (seconds)

pH of Rich AMP aqueous solution at different times (seconds)

I- Case B.2.1
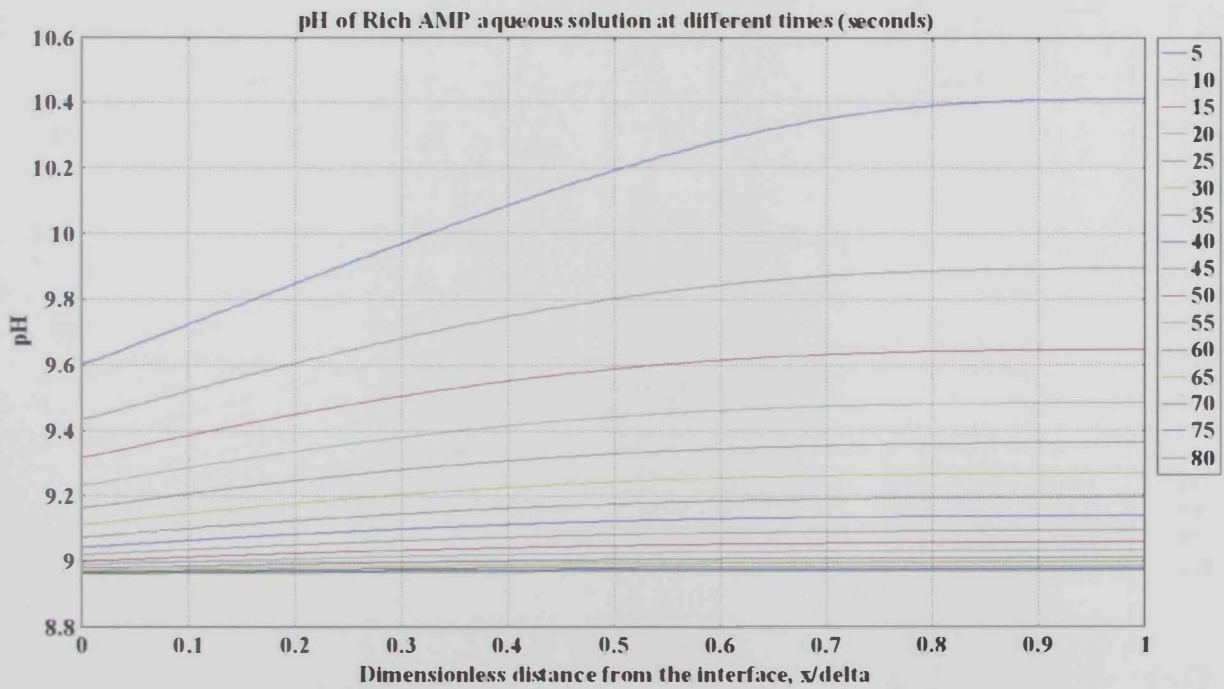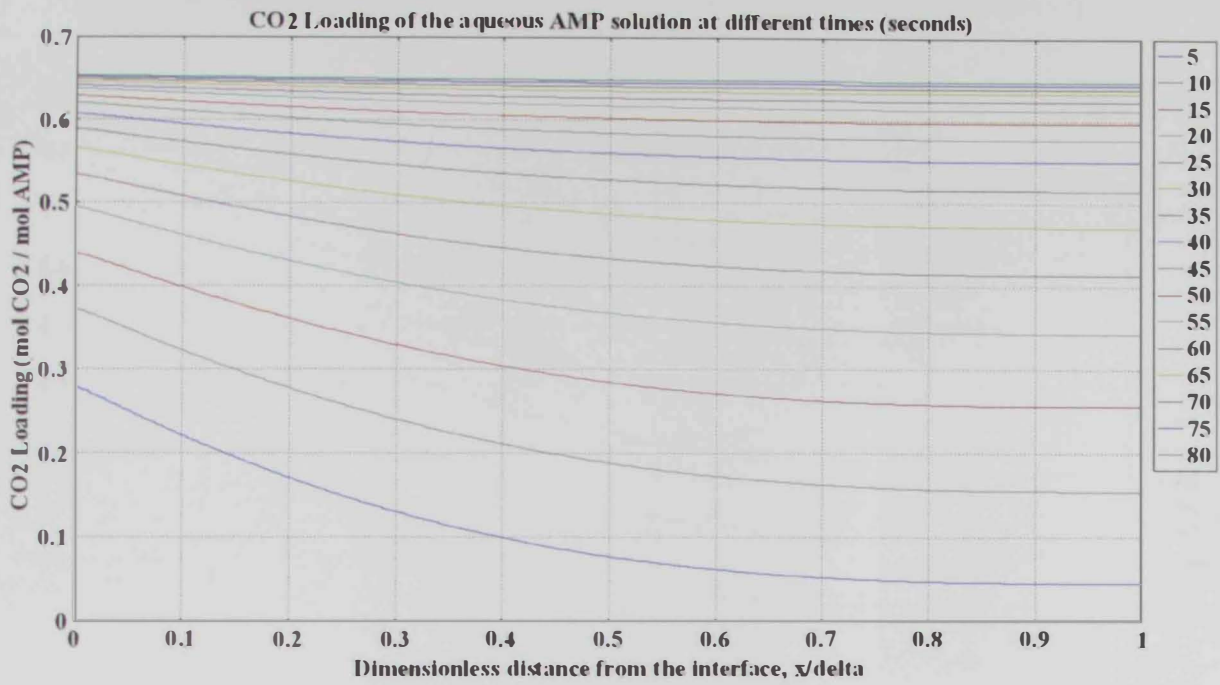

CO2 Loading of the aqueous AMP solution at different times (seconds)

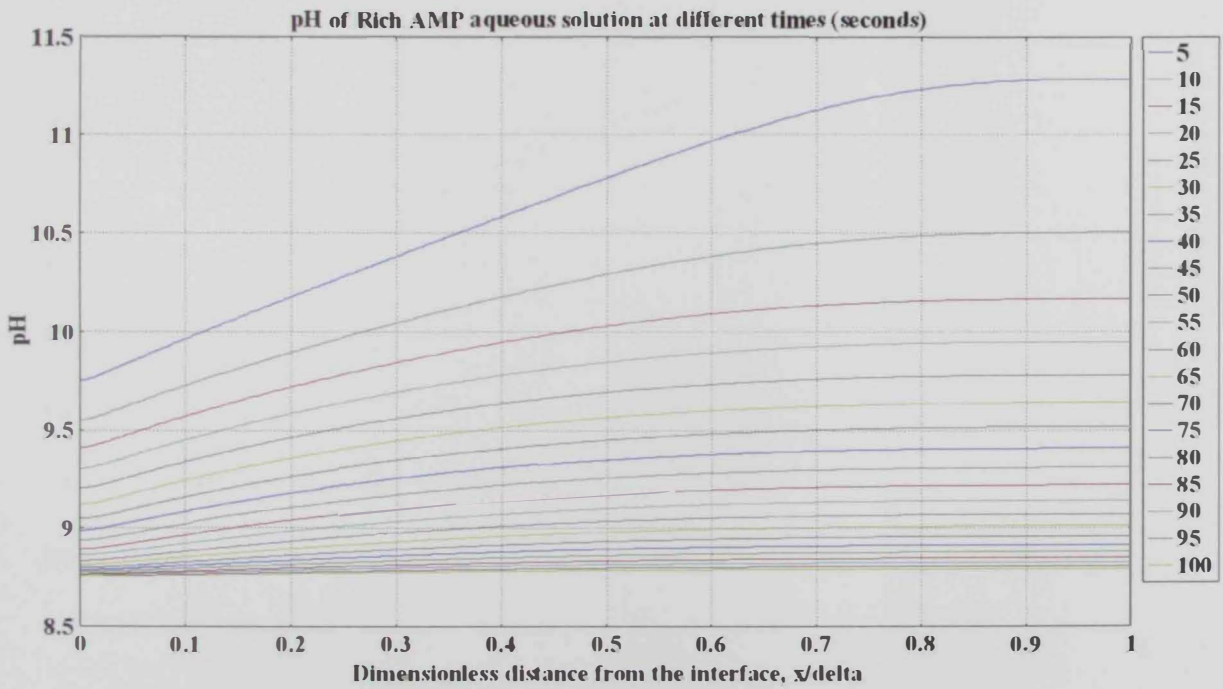pH of Rich AMP aqueous solution at different times (seconds)

I- Case B.2.2

CO2 Loading of the aqueous AMP solution at different times (seconds)

pH of Rich AMP aqueous solution at different times (seconds)

CO2 Loading of the aqueous AMP solution at different times (seconds)

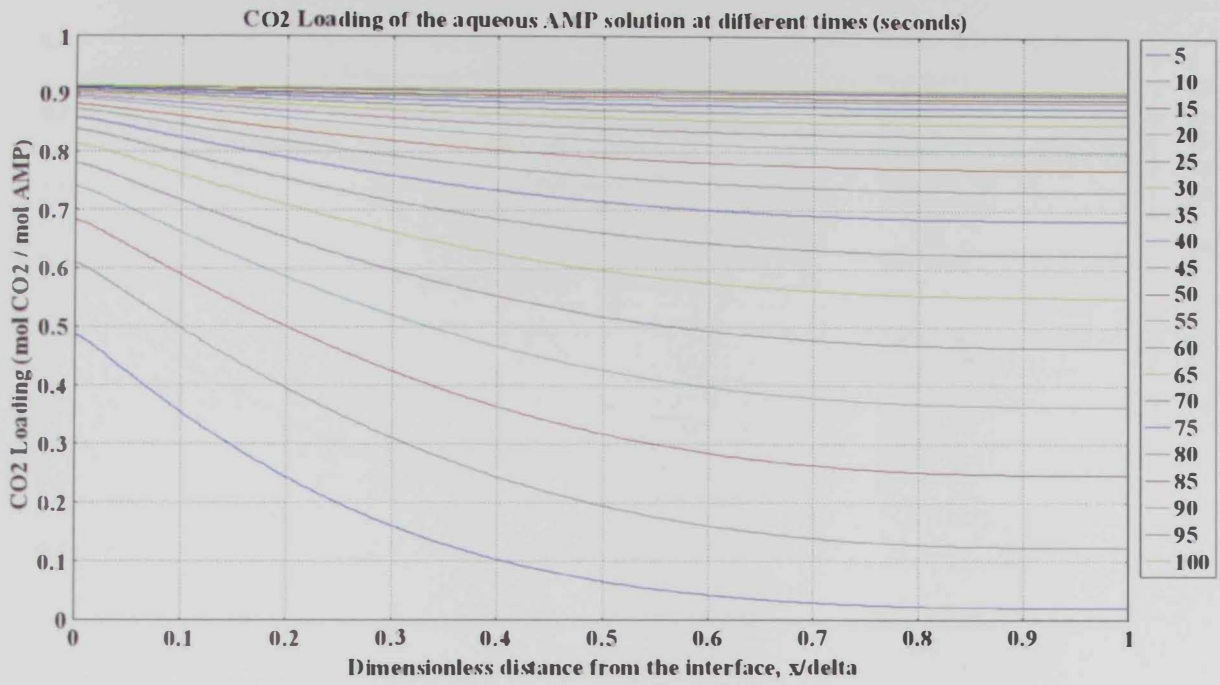pH of Rich AMP aqueous solution at different times (seconds)

I- Case B.3.2

CO2 Loading of the aqueous AMP solution at different times (seconds)

pH of Rich AMP aqueous solution at different times (seconds)

I- Case B.4.1

CO2 Loading of the aqueous AMP solution at different times (seconds)

pH of Rich AMP aqueous solution at different times (seconds)

I- Case B.4.2

CO2 Loading of the aqueous AMP solution at different times (seconds)

pH of Rich AMP aqueous solution at different times (seconds)

I- Case C.1.1

CO2 Loading of the aqueous AMP solution at different times (seconds)

pH of Rich AMP aqueous solution at different times (seconds)

I- Case C.1.2

CO2 Loading of the aqueous AMP solution at different times (seconds)

pH of Rich AMP aqueous solution at different times (seconds)

I- Case C.2.1

CO2 Loading of the aqueous AMP solution at different times (seconds)

pH of Rich AMP aqueous solution at different times (seconds)

I- Case C.2.2

CO2 Loading of the aqueous AMP solution at different times (seconds)

Y-axis: CO2 Loading (mol CO2 / mol AMP)
X-axis: Dimensionless distance from the interface, x/delta

Legend: 5, 10, 15, 20, 25, 30, 35, 40, 45, 50, 55, 60, 65, 70, 75, 80

pH of Rich AMP aqueous solution at different times (seconds)

Y-axis: pH
X-axis: Dimensionless distance from the interface, x/delta

Legend: 5, 10, 15, 20, 25, 30, 35, 40, 45, 50, 55, 60, 65, 70, 75, 80

I- Case C.3.1

CO2 Loading of the aqueous AMP solution at different times (seconds)

pH of Rich AMP aqueous solution at different times (seconds)

I- Case C.3.2

CO2 Loading of the aqueous AMP solution at different times (seconds)

pH of Rich AMP aqueous solution at different times (seconds)

I- Case C.4.1

CO2 Loading of the aqueous AMP solution at different times (seconds)

pH of Rich AMP aqueous solution at different times (seconds)

I- Case C.4.2

CO2 Loading of the aqueous AMP solution at different times (seconds)

pH of Rich AMP aqueous solution at different times (seconds)

APPENDIX B: OPERATING CASES (II) OF BOILER

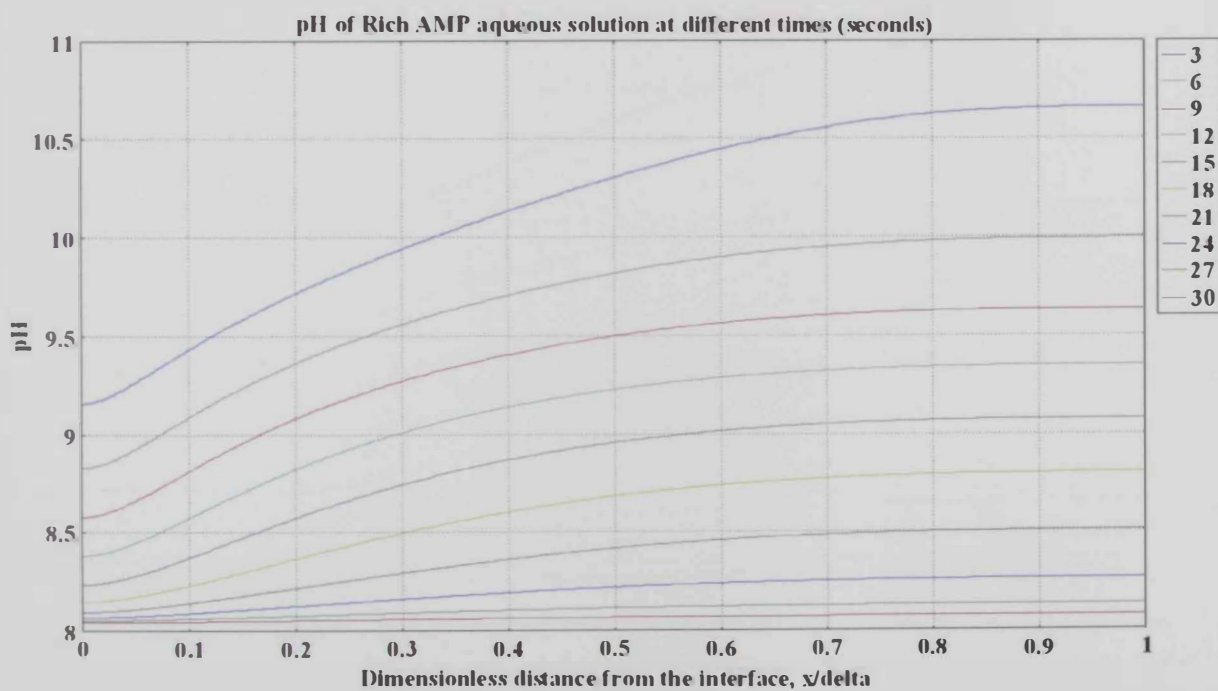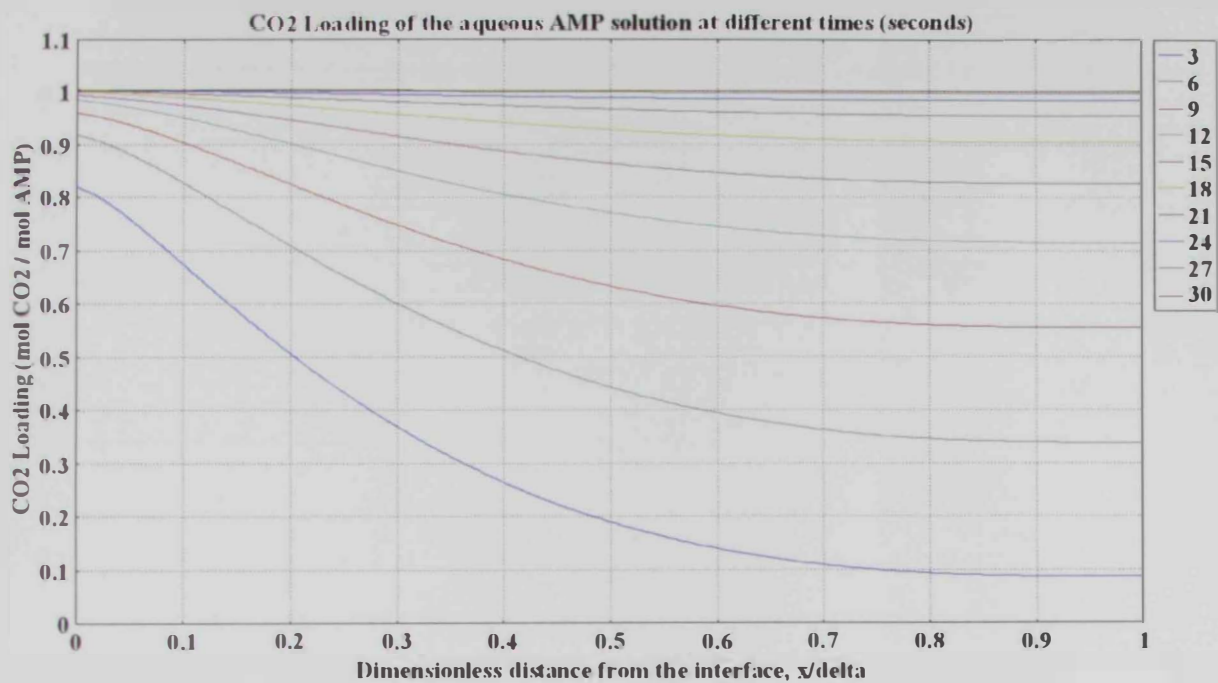This appendix displays the results for boiler cases. The code names are defined in Table 5.2-B.
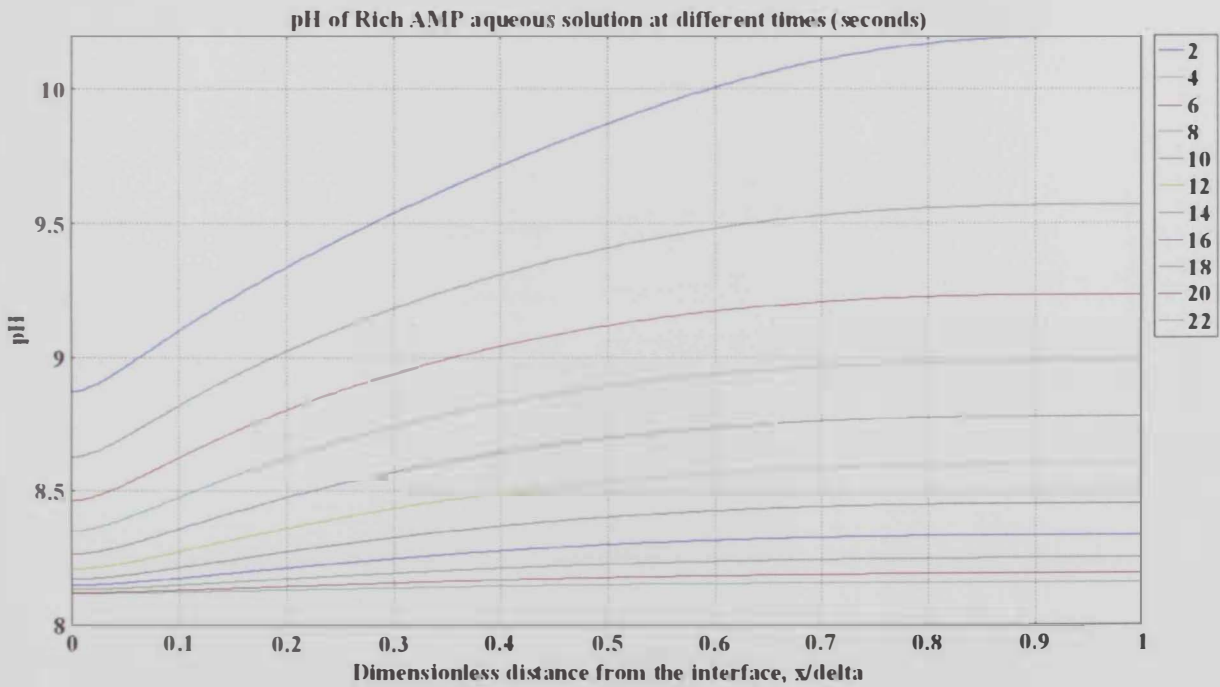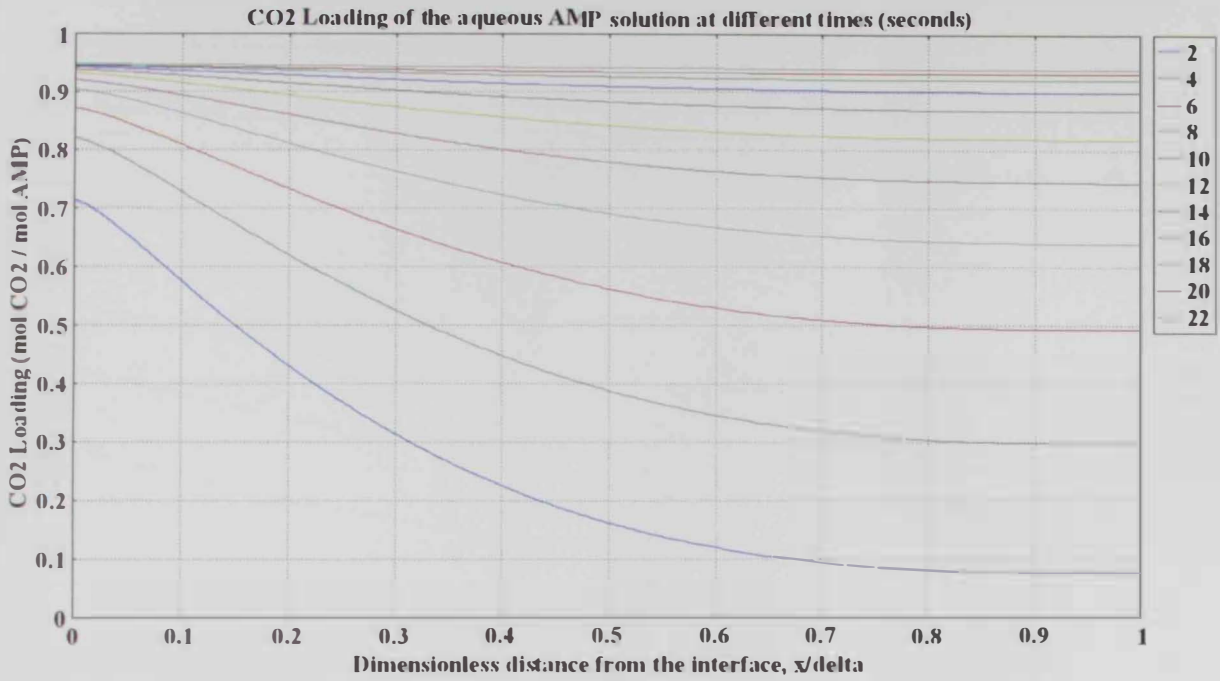
11- Case A.1.1

CO2 Loading of the aqueous AMP solution at different times (seconds)

pH of Rich AMP aqueous solution at different times (seconds)

II- Case A.1.2

CO2 Loading of the aqueous AMP solution at different times (seconds)

pH of Rich AMP aqueous solution at different times (seconds)

II- Case A.2.1

CO2 Loading of the aqueous AMP solution at different times (seconds)

pH of Rich AMP aqueous solution at different times (seconds)

II- Case A.2.2

CO2 Loading of the aqueous AMP solution at different times (seconds)

pH of Rich AMP aqueous solution at different times (seconds)

II- Case B.1.1

CO2 Loading of the aqueous AMP solution at different times (seconds)

Y-axis: CO2 Loading (mol CO2 / mol AMP)

X-axis: Dimensionless distance from the interface, x/delta

Legend: 10, 20, 30, 40, 50, 60, 70, 80, 90, 100, 110, 120, 130, 140, 150, 160

pH of Rich AMP aqueous solution at different times (seconds)

Y-axis: pH

X-axis: Dimensionless distance from the interface, x/delta

Legend: 10, 20, 30, 40, 50, 60, 70, 80, 90, 100, 110, 120, 130, 140, 150, 160

II- Case B.1.2

CO2 Loading of the aqueous AMP solution at different times (seconds)

pH of Rich AMP aqueous solution at different times (seconds)

11- Case B.2.1

CO2 Loading of the aqueous AMP solution at different times (seconds)

pH of Rich AMP aqueous solution at different times (seconds)

II- Case B.2.2

CO2 Loading of the aqueous AMP solution at different times (seconds)

pH of Rich AMP aqueous solution at different times (seconds)

II- Case C.1.1

CO2 Loading of the aqueous AMP solution at different times (seconds)

CO2 Loading (mol CO2 / mol AMP)

Dimensionless distance from the interface, x/delta

Legend: 15, 30, 45, 60, 75, 90, 105, 120, 135, 150, 165, 180, 195, 210, 225, 240

pH of Rich AMP aqueous solution at different times (seconds)

pH

Dimensionless distance from the interface, x/delta

Legend: 15, 30, 45, 60, 75, 90, 105, 120, 135, 150, 165, 180, 195, 210, 225, 240

II- Case C.1.2

CO2 Loading of the aqueous AMP solution at different times (seconds)

pH of Rich AMP aqueous solution at different times (seconds)

II- Case C.2.1

CO2 Loading of the aqueous AMP solution at different times (seconds)

pH of Rich AMP aqueous solution at different times (seconds)

II- Case C.2.2

CO2 Loading of the aqueous AMP solution at different times (seconds)

Y-axis: CO2 Loading (mol CO2 / mol AMP)
X-axis: Dimensionless distance from the interface, x/delta

Legend: 5, 10, 15, 20, 25, 30, 35, 40, 45, 50, 55, 60

pH of Rich AMP aqueous solution at different times (seconds)

Y-axis: pH
X-axis: Dimensionless distance from the interface, x/delta

Legend: 5, 10, 15, 20, 25, 30, 35, 40, 45, 50, 55, 60